The contribution of oceanic halocarbons to marine and free troposphere air over the tropical West Pacific

S. Fuhlbrügge[1], B. Quack[1], S. Tegtmeier[1], E. Atlas[2], H. Hepach[1], Q. Shi[3], S. Raimund[1], K. Krüger[4]

[1] GEOMAR - Helmholtz Centre for Ocean Research Kiel, Kiel, Germany

[2] Rosenstiel School for Marine and Atmospheric Sciences, Miami, Florida

[3] Department of Oceanography - Dalhousie University, Halifax, Canada

[4] University of Oslo, Oslo, Norway

Correspondence to: K. Krüger (kirstin.krueger@geo.uio.no)

Response to Editor

Editor:

Comments to the Author:

Dear authors,

as discussed in our separate email discussion and according to your question in the answer to my latest review, you wish to resubmit another revised manuscript. I am calling this a minor revision, since I need to review it again.

kind regards

Michael

Authors:

We thank the editor that he agreed with our suggestions in the reply to the previous editor report. Below you find a list with relevant changes and the revised manuscript including the improved method to compute free troposphere VSLS mixing ratios.

Relevant changes in the manuscript

- Adjusted signs in Eq. 3 – 6 and Table 3 to simplify and visualise the mass balance equations (source / loss processes) and to be consistent with the current review of Fuhlbrügge et al. 2015. This didn't affect the results.
- Added dependencies of variables in Eq. 11 and 12
- Replaced Eq.13 with the new method.
- Removed box approach and Figure 8.
- Updated results in 5.3.1 – 5.3.3, 6. according to the new method (Eq. 13).
- Updated former Figure 10, now 9 without box approach.
- Updated former Figure 11, now 10 using new method (Eq. 13).

References

Fuhlbrügge, S., Quack, B., Atlas, E., Fiehn, A., Hepach, H., and Krüger, K.: Meteorological constraints on oceanic halocarbons above the Peruvian Upwelling, Atmos. Chem. Phys. Discuss., 15, 20597–20628, 10.5194/acpd-15-20597-2015, 2015.

The contribution of oceanic halocarbons to marine and free troposphere air over the tropical West Pacific

S. Fuhlbrügge[1], B. Quack[1], S. Tegtmeier[1], E. Atlas[2], H. Hepach[1], Q. Shi[3], S. Raimund[1], K. Krüger[4]

[1] GEOMAR - Helmholtz Centre for Ocean Research Kiel, Kiel, Germany

[2] Rosenstiel School for Marine and Atmospheric Sciences, Miami, Florida

[3] Department of Oceanography - Dalhousie University, Halifax, Canada

[4] University of Oslo, Oslo, Norway

Correspondence to: K. Krüger (kirstin.krueger@geo.uio.no)

Abstract

Emissions of halogenated very short lived substances (VSLS) from the oceans contribute to the atmospheric halogen budget and affect tropospheric and stratospheric ozone. Here, we investigate the contribution of natural oceanic VSLS emissions to the Marine Atmospheric Boundary Layer (MABL) and their transport into the Free Troposphere (FT) over the tropical West Pacific. The study concentrates on bromoform, dibromomethane and methyl iodide measured on ship and air craft during the SHIVA (Stratospheric Ozone: Halogen Impacts in a Varying Atmosphere) campaign in the South China and Sulu Seas in November 2011. Elevated oceanic concentrations for bromoform, dibromomethane and methyl iodide of on average 19.9, 5.0 and 3.8 pmol L^{-1} in particular close to Singapore and at the coast of Borneo with high corresponding oceanic emissions of 1486, 405 and 433 pmol m^{-2} h^{-1}, respectively, characterize this tropical region as a strong source of these compounds. Atmospheric mixing ratios in the MABL were unexpectedly relatively low with 2.08, 1.17 and 0.39 ppt for bromoform, dibromomethane and methyl iodide. We use meteorological and chemical ship and aircraft observations, FLEXPART trajectory calculations and source-loss estimates to identify the oceanic VSLS contribution to the MABL and to the FT. Our results show that the well-ventilated MABL and intense convection led to the low atmospheric mixing ratios in the MABL despite the high oceanic emissions. Up to 45 % of the accumulated bromoform in the FT above the region originates from the local South China Sea area, while dibromomethane is largely advected from distant source regions and the local ocean only contributes 20 %. The accumulated methyl iodide in the FT is higher than can be explained with local

contributions. Possible reasons, uncertainties and consequences of our observations and model estimates are discussed.

1. Introduction

Halogens play an important role for atmospheric chemical processes. Chlorine, bromine and iodine radicals destroy ozone in the stratosphere (e.g. Solomon, 1999) and also affect tropospheric chemistry (e.g. Saiz-Lopez and von Glasow, 2012). Halogens are released following the photochemical breakdown of organic anthropogenic and natural trace gases. A large number of very short lived brominated and iodinated organic substances, originating from macro algae, seaweed, phytoplankton and other marine biota, are emitted from tropical oceans and coastal regions to the atmosphere (Gschwend et al., 1985;Carpenter and Liss, 2000;Quack and Wallace, 2003;Quack et al., 2007;Liu et al., 2013). In particular, marine emissions of bromoform ($CHBr_3$), dibromomethane (CH_2Br_2) and methyl iodide (CH_3I) are major contributors of bromine and iodine to the atmosphere (Montzka and Reimann, 2011). Annually averaged mean tropical lifetimes of these halogenated very short-lived substances (VSLS) in the boundary layer are 15 (range: 13 – 17) days for $CHBr_3$, 94 (84 – 114) days for CH_2Br_2 and 4 (3.8 – 4.3) days for CH_3I. The mean tropospheric lifetimes of these compounds at 10 km height are 17 (16 – 18) days, 150 (144 – 155) days, respectively 3.5 (3.4 – 3.6) days (Carpenter et al., 2014). Climate change could strongly affect marine biota and thereby halogen sources and the oceanic emission strength (Hughes et al., 2012;Leedham et al., 2013;Hepach et al., 2014).

Aircraft measurements from Dix et al. (2013) suggest that the halogen-driven ozone loss in the Free Troposphere (FT) is currently underestimated. In particular, elevated amounts of the iodine oxide free radical (IO) in the FT over the Central Pacific indicate that iodine may have a larger effect on the FT ozone budget than currently estimated by chemical models. Coinciding with this study, Tegtmeier et al. (2013) projected a higher CH_3I delivery to the Upper Troposphere / Lower Stratosphere (UTLS) over the tropical West Pacific than previously reported, using an observation based emission climatology by Ziska et al. (2013). Recent studies reported significant contributions of bromine and iodine to the total rate of tropospheric and stratospheric ozone loss (e.g. von Glasow et al., 2004;Yang et al., 2005;Saiz-Lopez et al., 2014;Yang et al., 2014;Hossaini et al., 2015). Deep tropical convective events (Aschmann et al., 2011;Tegtmeier et al., 2013;Carpenter et al., 2014) as well as tropical cyclones, i.e. typhoons (Tegtmeier et al., 2012), are projected to transport VSLS rapidly from the ocean surface to the upper tropical tropopause layer. Despite the

importance of halogens on tropospheric and stratospheric ozone chemistry, halogen sources and transport ways are still not fully understood. While the tropical West Pacific comprises strong VSLS source regions (Krüger and Quack, 2013), only low mean atmospheric mixing ratios were observed during ship campaigns in 1994 and 2009 (Yokouchi et al., 1997;Quack and Suess, 1999) and in 2010 (Quack et al., 2011;Brinckmann et al., 2012). None of these previous studies investigated the contribution of oceanic VSLS emissions to the marine atmospheric boundary layer (MABL) and to the FT in this hot spot region with large oceanic sources and strong convective activity.

The SHIVA ('Stratospheric Ozone: Halogen Impacts in a Varying Atmosphere') ship, aircraft and ground-based campaign during November and December 2011 in the Southern South China and Sulu Seas investigated oceanic emission strengths of marine VSLS, as well as their atmospheric transport and chemical transformation from the ocean surface to the upper troposphere. For more details about the SHIVA campaign see the ACP special issue (http://www.atmos-chem-phys.net/special_issue306.html).

In this study, we present campaign data from the research vessel (R/V) SONNE and the research aircraft (R/A) FALCON. We identify the contribution of oceanic emissions to the MABL and their exchange into the FT applying in-situ observations, trajectory calculations and source-loss estimates. The results are crucial for a better process understanding and for chemical transport model validation (Hossaini et al., 2013;Aschmann and Sinnhuber, 2013). An overview of the data and the methods used in this study is given in Chapter 2. Chapter 3 provides results from the meteorological observations along the cruise. Chapter 4 compares atmospheric VSLS measurements derived on R/V SONNE and R/A FALCON. The contribution of the oceanic emissions to the MABL and FT air is investigated and discussed in Chapter 5. Finally, a summary of the results is given in Chapter 6.

2. Data and Methods

2.1. Ship and aircraft campaigns

The R/V SONNE cruise started on November 15, 2011 in Singapore and ended on November 29, 2011 in Manila, Philippines (Figure 1). The ship crossed the southwestern South China Sea towards the northwestern coast of Borneo from November 16 – 19, 2011. From November 19 - 23, 2011 the ship headed northeast along the northern coast of Borneo towards the Sulu Sea. Two diurnal stations took place on November 18, 2011 at 2.4° N / 110.6° E and on November 22, 2011 at 6.0° N / 114.8° E. Two meetings between ship and aircraft were carried out on November 19 and 21, 2011, where R/A FALCON passed R/V

SONNE within a distance of about 100 m several times to simultaneously measure the same air masses. On November 24, 2011 the ship entered the Sulu Sea, and after 4 days transect, R/V SONNE reached the Philippine coast.

16 measurement flights were carried out with R/A FALCON between November 16 and December 11, 2011 as part of the SHIVA campaign to investigate halogenated VSLS from the surface up to 13 km altitude over the South China and Sulu Seas. Observations were performed between 1° N and 8° N, as well as 100° E and 122° E, from Miri, Borneo (Malaysia) as the aircraft base. A detailed description of the VSLS measurements and flight tracks can be found in Sala et al. (2014).

2.2. Meteorological observations during SHIVA

2.2.1. Measurements on board R/V SONNE

Meteorological parameters (temperature, air pressure, humidity and wind) were recorded at 20 m height every second. A 10 minute running mean of this data is used for this study. An optical disdrometer ('ODM-470') measured the amount and intensity of precipitation during the cruise at 15 m height every minute (see Supplementary Material for further details). To obtain atmospheric profiles of air temperature, relative humidity and wind from the surface to the stratosphere 67 GRAW DFM-09 and 6 GRAW DFM-97 radiosondes were launched every 6 hours at standard UTC times (0, 6, 12, 18) from the working deck of R/V SONNE at about 2 m above sea level. At the 24 h stations, the launch frequency was increased to 2 – 3 hours to analyse short term diel variations of the atmospheric boundary layer. The radiosonde data was integrated in near real time into the Global Telecommunication System (GTS) to improve meteorological reanalyses such as ERA-Interim (Dee et al., 2011), which is used as input data for the trajectory calculations (Section 5).

2.2.2. Marine atmospheric boundary layer

The MABL is the atmospheric surface layer above the ocean in which trace gas emissions are mixed vertically by convection and turbulence on a short time scale of about an hour (Stull, 1988;Seibert et al., 2000). The upper boundary of the MABL is either indicated by a stable layer e.g. a temperature inversion or by a significant reduction in air moisture. Determination of the MABL height can be achieved by theoretical approaches, e.g. using critical Bulk Richardson number (Troen and Mahrt, 1986;Vogelezang and Holtslag, 1996;Sorensen, 1998) or by practical approaches summarized in Seibert et al. (2000). An increase with height of the virtual potential temperature, the temperature an air parcel would acquire if adiabatically

brought to standard surface pressure with regard to the humidity of the air parcel, identifies the base of the stable layer, which is typically found between 100 m and 3 km altitude (Stull, 1988). In this study, we use the height of the base of the stable layer increased by half of the stable layer depth as the definition for the MABL height. The height of the MABL is determined from the atmospheric profiles measured by radiosondes launched on board the ship, as described in detail by Fuhlbrügge et al. (2013).

2.3. VSLS measurements and flux calculation

VSLS in marine surface air and sea water were sampled synchronously on R/V SONNE along the cruise track. From these data the oceanic emissions of the compounds during the SHIVA campaign were calculated (Section 2.3.3). Additionally, VSLS were measured in the MABL and the FT by R/A FALCON (Sala et al., 2014;Tegtmeier et al., 2013).

2.3.1. Atmospheric samples

Air samples were taken 3 hourly along the cruise track, and 1 – 2 hourly during the 24 hour stations on R/V SONNE resulting in a total of 195 samples during the cruise. The air was pressurized to 2 atm in pre-cleaned stainless steel canisters with a metal bellows pump. The samples were analyzed within 6 months after the cruise at the Rosenstiel School for Marine and Atmospheric Sciences (RSMAS, Miami, Florida) according to Schauffler et al. (1999) with an instrumental precision of ~5 %. Further details of the analysis are described in Montzka et al. (2003) and Fuhlbrügge et al. (2013). On R/A FALCON ambient air was analysed in situ by a GhOST-MS (Gas Chromatograph for the Observation of Stratospheric Tracers – coupled with a Mass Spectrometer) by the Goethe University of Frankfurt (GUF). Additionally 700 ml glass flasks were filled with ambient air to a pressure of 2.5 bar with the R/A FALCON whole air sampler (WASP) and analysed within 48 hours by a ground-based gas chromatography – mass spectrometry (GC/MS) instrument (Agilent 6973) of the University of East Anglia (Worton et al., 2008). During the flights GhOST measurements were conducted approximately every 5 minutes with a sampling time of 1 minute, while WASP samples were taken every 3 – 15 minutes with a sampling time of 2 minutes. Further details on the instrumental precision and intercalibration on R/A FALCON are given in Sala et al. (2014). Given that the ground-based GC/MS investigated only brominated compounds, CH_3I data is not available from WASP. Measurements from R/V SONNE and R/A FALCON were both calibrated with NOAA standards.

2.3.2. Water samples

VSLS sea water samples were taken 3 hourly from the moon pool of R/V SONNE at a depth of 5 m from a continuously working water pump. Measurements were interrupted between November 16, 00 UTC to November 17, 2011 12 UTC due to permission issues in the southwest South China Sea. The water samples were analysed on board with a purge and trap system, attached to a gas chromatograph with mass spectrometric detection in single-ion mode and a precision of 10 % determined from duplicates. The method is described in detail by Hepach et al. (2014).

2.3.3. Sea – air flux

The sea – air flux (F) of $CHBr_3$, CH_2Br_2 and CH_3I is calculated with k_w the concentration gradient, and Δc the concentration gradient between the water and atmospheric equilibrium concentrations (Eq. 1). For the determination of k_w, the wind speed-based parameterization of Nightingale et al. (2000) was used and a Schmidt number (Sc) correction to the carbon dioxide derived transfer coefficient k_{CO_2} after Quack and Wallace (2003) was applied for the three gases (Eq. 2).

$$F = k_w \cdot \Delta c \quad \text{(Eq. 1)}$$

$$k_w = k_{CO_2} \cdot \frac{Sc^{-\frac{1}{2}}}{600} \quad \text{(Eq. 2)}$$

Details on measuring the air – sea concentration gradient are further described in Hepach et al. (2014) and references therein.

2.4. Oceanic VSLS contribution to the MABL and FT

2.4.1. Trajectory calculations

The air mass transport from the surface to the FT was calculated with the Lagrangian Particle Dispersion Model FLEXPART from the Norwegian Institute for Air Research in the Department of Atmospheric and Climate Research (Stohl et al., 2005). The model has been extensively evaluated in earlier studies (Stohl et al., 1998;Stohl and Trickl, 1999) and includes parameterizations for turbulence in the atmospheric boundary layer and the FT as well as moist convection (Stohl and Thomson, 1999;Forster et al., 2007). Meteorological

input fields are retrieved from the ECMWF (European Centre for Medium-Range Weather Forecasts) assimilation reanalysis product ERA-Interim (Dee et al., 2011) with a horizontal resolution of 1° x 1° and 60 vertical model levels. The ship-based 6 hourly radiosonde measurements were assimilated into the ERA-Interim data (Section 2.2.1) and provide air temperature, horizontal and vertical wind, boundary layer height, specific humidity, as well as convective and large scale precipitation. For the trajectory analysis, 80 release points were defined along the cruise track. Time and position of these release events are synchronized with the water and air samples (Section 2.3). At each event, 10,000 trajectories were launched from the ocean surface within a time frame of ± 30 minutes and an area of ~400 m^2.

2.4.2. VSLS source-loss estimate in the MABL

The time scales of air mass transport derived from FLEXPART together with the oceanic emissions and chemical losses of the VSLS are used for a mass balance source-loss estimate over the South China and Sulu Seas. For each release event, a box given by the in-situ height of the MABL and by the horizontal area of the trajectory releases (~400 m^2 centred on the measurement location) is defined. The MABL source-loss estimate is based on the assumption of a constant VSL S mixing ratio (given by the atmospheric measurements), a constant sea – air flux, the chemical loss rate, and a VSLS homogeneous distribution with the box during each release.

The Oceanic Delivery (OD) is given as the contribution of VSLS sea – air flux (in mol per day) to the total amount of the VSLS in the box (in mol) in percentage per day. The loss of MABL air to the FT caused by vertical transport, denoted here Convective Loss (COL), is calculated from the mean residence time of the FLEXPART trajectories in the observed MABL during each release and is given as a negative number in percentage per day. COL equals the loss of VSLS from the MABL to the FT. The Chemical Loss (CL), in the form of reaction with OH and photolysis, is estimated in percentage per day (negative quantity) and is based on the tropical MABL lifetime estimates of 15 days for $CHBr_3$, 94 days for CH_2Br_2 and 4 days for CH_3I (Carpenter et al., 2014).

Relating the delivery of VSLS from the ocean to the MABL (OD) and the loss of MABL air containing VSLS to the FT (COL) results in an Oceanic Delivery Ratio (ODR) (Eq. 3):

$$ODR = \frac{OD\ [\%d^{-1}]}{-COL\ [\%d^{-1}]} = \frac{Sea{-}Air\ flux\ contribution\ [\%d^{-1}]}{Loss\ of\ MABL\ air\ to\ the\ FT\ [\%d^{-1}]} \quad \text{(Eq. 3)}$$

Similarly, the Chemical Loss in the MABL (CL) related to the MABL VSLS loss into the FT (COL) leads to a Chemical Loss Ratio (CLR) (Eq. 4):

$$CLR = \frac{CL\ [\%d^{-1}]}{-COL\ [\%d^{-1}]} = \frac{Loss\ through\ chemistry\ [\%d^{-1}]}{Loss\ of\ MABL\ air\ to\ the\ FT\ [\%d^{-1}]} \quad \text{(Eq. 4)}$$

The oceanic delivery, chemical loss and loss to the FT must be balanced by advective transport of air masses in and out of the box. We define the change of the VSLS through advective transport as Advective Delivery (AD) in percentage per day (Eq. 5). Additionally, we define the ratio of change in VSLS caused by advection (AD) to the loss of VSLS out of the MABL to the FT as Advective Delivery Ratio (ADR) in Eq. 6:

$$AD = -COL \mp CL - OD \quad \text{(Eq. 5)}$$

$$ADR = \frac{AD\ [\%d^{-1}]}{-COL\ [\%d^{-1}]} = 1 \mp CLR - ODR \quad \text{(Eq. 6)}$$

Note that for the VSLS within the MABL box, COL and CL are loss processes ~~and given as negative numbers~~ while OD and AD (besides very few exceptions for the latter) are source processes~~ and given as positive numbers~~. In order to derive the ratios, we divided CL, OD and AD by COL~~ and therefore end up with negative ratios for the loss process and positive ratios for the source processes~~.

In a final step, we relate the source-loss ratios (ODR, CLR and ADR) to the MABL VSLS volume mixing ratio VMR_{MABL} in the box (Eq. 7 – 9), in order to estimate VSLS newly supplied from oceanic delivery (VMR_{ODR}), lost by chemical processes (VMR_{CLR}) and supplied by advective transport (VMR_{ADR}).

$$VMR_{ODR} = ODR \cdot VMR_{MABL} \quad \text{(Eq. 7)}$$

$$VMR_{CLR} = CLR \cdot VMR_{MABL} \quad \text{(Eq. 8)}$$

$$VMR_{ADR} = ADR \cdot VMR_{MABL} \quad \text{(Eq. 9)}$$

2.4.3. Oceanic and MABL VSLS contribution to the FT

We use a simplified approach to calculate the mean contribution of boundary layer air masses observed from various oceanic regions in the South China Sea on the ship, and the oceanic compounds therein, to the FT above the South China and Sulu Seas. The contribution is

determined as a function of time and altitude based on the distribution of the trajectories released at each measurement location along the ship track. According to R/A FALCON observations and our trajectory calculations we assume a well-mixed FT ~~within 5° S - 20° N, 100° E – 125° E~~. Observations on R/V SONNE, on the other hand, are characterized by large variability and are considered to be representative for the area along the cruise track where the VSLS were measured in the water and atmosphere. We constrain our calculations to this area and define 80 vertical columns along the cruise track. Each column extends horizontally over the area given by the starting points of the trajectories (20 m x 20 m centred on the measurement location) and vertically from the sea surface up to the highest point of R/A FALCON observations around 13 km altitude. For each of the 80 columns along the cruise track, 10,000 trajectories were launched and assigned an identical MABL air parcel containing air with the VSLS mixing ratios observed on R/V SONNE during the time of the trajectory release. The volume of the air parcel is given by the in-situ height of the MABL and the horizontal extent of the release box (20 m x 20 m) divided by 10,000 trajectories. The transport of the MABL air parcels is specified by the trajectories, assuming that no mixing occurs between the parcels during the transport. Chemical loss of the VSLS in each air parcel is taken into account through chemical degradation according to their specific tropospheric lifetimes. The VSLS mixing ratios in the FT from the aircraft measurements are considered representative for the whole South China Sea area. Thus we average over the volume and mixing ratios of all trajectories within the South China Sea area, independent of their exact horizontal location. Due to the decreasing density of air in the atmosphere with height, the volume of the MABL air parcels expands along the trajectories with increasing altitude. The expanding MABL air parcels take up an increasing fraction of air within the FT column, which is taken into account in our calculations using density profiles from our radiosonde measurements.

We calculate the contribution of oceanic compounds to the FT ~~for 25 layers of 500 m height intervals between 0.5 km and~~up to 13 km altitude, the upper height of R/A FALCON observations, within the column above the measurement location. For each layer, the ratio r_{MABL} of the volume of the MABL air parcels with the VSLS mixing ratio VMR_{MABL} to the whole air volume of the layer is calculated. The ratio of advected FT air with a mixing ratio VMR_{AFT} to the whole air volume of the layer is r_{AFT}, respectively, with $r_{MABL} + r_{AFT} = 1$. In our simulation, the FT air with a mixing ratio VMR_{FT} observed by R/A FALCON at a specific height is composed of the MABL air parcels and of the advected FT air parcels (Eq. 10):

$$r_{MABL} \cdot VMR_{MABL} + r_{AFT} \cdot VMR_{AFT} = (r_{MABL} + r_{AFT}) \cdot VMR_{FT} \quad \text{(Eq. 10)}$$

The relative contribution C_{MABL} of VSLS observed in the MABL to the VSLS observed in the FT at height z and time t is computed in altitude steps of 500 m (Eq. 11):

$$C_{MABL}(z,t)[\%] = 100 \cdot (r_{MABL}(z,t) \cdot VMR_{MABL}(CL(t)))/VMR_{FT}(z) \quad \text{(Eq. 11)}$$

The oceanic contribution C_{ODR} of the South China Sea emissions to the VSLS in the FT is computed after Eq. 12:

$$C_{ODR}(z,t)[\%] = 100 \cdot (r_{MABL}(z,t) \cdot VMR_{ODR}(CL(t)))/VMR_{FT}(z) \quad \text{(Eq. 12)}$$

The simplified approach also allows deriving mean VSLS mixing ratios accumulated in the FT from both MABL VSLS and oceanic emissions. The FT VSLS mixing ratios are simulated for each of the 80 columns by initiating a new trajectory release event using same meteorological conditions and VSLS MABL observations~~, when the former MABL air has been transported into the FT, according to the specific residence time in the MABL~~. ~~The initial FT background mixing ratios are 0 ppt for each VSLS.~~ The accumulated mean mixing ratio of a compound at a specific height z is then ~~computed~~ iterated after Eq. 13:

~~$$VMR_{MFT} = r_{MABL_1} \cdot VMR_{MABL_1} + r_{MABL_2} \cdot VMR_{MABL_2} + \ldots + r_{MABL_t} \cdot VMR_{MABL_t}$$~~ ~~(Eq. 13)~~

$$VMR_{FT}(z) = \sum_{i=1}^{n} \begin{pmatrix} r_{MABL}(z,t(i)) \cdot VMR_{MABL}\left(CL(t(i))\right) \\ + \\ \left(1 - r_{MABL}(z,t(i))\right) \cdot VMR_{FT}(z,t(i-1)) \cdot CL(COL) \end{pmatrix} \quad \text{(Eq. 13)}$$

Here, n is the number of runs for each of the 80 profiles, according to the residence time of the trajectories in the MABL and the total runtime of the trajectories. For example a trajectory residence time of 7 hours in the MABL in combination with a total trajectory runtime of 16 days leads to n = (24 / 7) * 16 = 54. r_{MABL} gives the volume ratio of MABL air parcels at height z and time t to the total volume of a specific height layer. VMR_{MABL} gives the compounds mixing ratio in the air parcels including chemical degradation (CL) since the air was observed in the MABL. Since we use a mean tropospheric lifetime, CL and thus also

VMR_{MABL}(CL) are independent from the height *z*. The initial FT background mixing ratios ($VMR_{FT}(z,t(i=0))$) are set to 0 ppt for each VSLS, followed by *n* times iteration of $VMR_{FT}(i-1)$. The difference between $VMR_{FT}(i = n-1)$ and $VMR_{FT}(i = n)$ during the last two steps of the iteration is less than 1 % for each compound within the 16 days runtime.

~~Here, VMR_{FT} is the modelled accumulated FT mixing ratio, r_{MABL_t} is the ratio of MABL air parcels in 20 m x 20 m x 500 m layers between 0.5 km and 13 km altitude to the total volume of each layer, VMR_{MABL_t} is the mixing ratio in the MABL air parcels including chemical degradation since release from the MABL, and *i* is the number of initiated runs per release. A steady state for the compounds is reached, when variations in their mixing ratios vary less than 1 % between two initiated runs. For $CHBr_3$ the steady state is reached after 11.0 ± 2.1 d (mean ± σ), 11.8 ± 2.4 d for CH_2Br_2 and 8.0 ± 1.4 d for CH_3I.~~ The modelled overall mean FT mixing ratio ~~in the South China Sea~~ is derived as the mean from the 80 individually calculated FT mixing ratios determined along the cruise. The oceanic contribution to the FT compounds is calculated with VMR_{ODR} from Eq. 7 inserted as VMR_{MABL} in Eq. 13.

3. Meteorological conditions in the MABL and the FT

3.1. Meteorology along the ship cruise

Moderate to fresh trade winds were dominating the South China and Sulu Seas during the cruise (Figure 1a-b), indicated by the overall mean wind direction of northeast (50° – 60°) and a mean wind speed of 5.5 ± 2.9 ms^{-1}. The wind observations reveal two different air mass origins. Between November 15 and 19, 2011 a gentle mean wind speed of 3.7 ± 1.8 ms^{-1} with a *northern* wind direction was observed, influenced by a weak low pressure system (not shown here) over the central South China Sea moving southwest and passing the ship position on 17.11.2011. During November 20 – 29, 2011 the wind direction changed to *northeast* and the mean wind speed increased to moderate 6.4 ± 3.0 ms^{-1}. A comparison between 6 hourly ERA-Interim wind and a 6 hourly averaged mean of the observed wind on R/V SONNE reveals an underestimation of the wind speed by ERA-Interim along the cruise track by 1.6 ± 1.4 ms^{-1} on average (not shown here). The mean deviation of the wind direction between reanalysis and observation is 2 ± 37 degree. Reanalysis and observed wind speeds correlate with R = 0.76 and the wind directions with R = 0.86, reflecting a good overall agreement between ship observation and ERA-Interim winds. With an observed mean surface air temperature (SAT) of 28.2 ± 0.8 °C and a mean SST of 29.1 ± 0.5 °C the SAT is on average 1.0 ± 0.7 °C below the SST, which benefits convection of surface air (Figure 2).

Indeed enhanced convective activity and pronounced precipitation events have been observed during the cruise (S-Figure 1). Figure 3a shows the time series of the relative humidity measured by the radiosondes launched on R/V SONNE from the surface up to the mean height of the cold point tropopause at 17 km. Elevated humidity is found on average up to about 6 km, which implies a distinct transport of water vapour to the mid troposphere during the cruise by deep convection or advection of humid air from a nearby convective cell.

3.2. Marine atmospheric boundary layer

Higher SSTs than SATs (Figure 2) cause unstable atmospheric conditions (negative values) between the surface and about 50 – 100 m height (Figure 3b). Surface air is heated by warmer surface waters and is enriched with humidity both benefiting moist convection. The stability of the atmosphere increases above 420 ± 120 m and indicates the upper limit of the MABL at this altitude range derived from radiosonde data (Figure 3b). The MABL height given by ERA-Interim along the cruise track is with 560 ± 130 m systematically higher (not shown), but still within the upper range of the MABL height derived from the radiosonde measurements. The unstable conditions of the MABL and the increase of the atmospheric stability above the MABL reflect the characteristics of a convective, well-ventilated tropical boundary layer. In contrast to cold oceanic upwelling regions with a stable and isolated MABL (Fuhlbrügge et al., 2013;Fuhlbrügge et al., 2015), the vertical gradient of the relative humidity measured by the radiosondes (Section 3.1) and the height of the MABL do not coincide. This is caused by increased mixing through and above the MABL by turbulence and convection, which leads to the convective, well-ventilated MABL.

4. Atmospheric VSLS over the South China and Sulu Seas

4.1. Atmospheric surface observations on R/V SONNE

Overall, the three VSLS show a similar pattern of atmospheric mixing ratios along the cruise track with lower atmospheric surface abundances before 21 November 2011 and higher concentrations afterwards, which can be attributed to a change in air mass origin (Figure 1). A decrease from 3.4 to 1.2 ppt of $CHBr_3$ occurs at the beginning of the cruise (Figure 4a) when the ship left Singapore and the coast of the Malaysian Peninsula. On November 16 – 19, 2011, when the ship passed the southern South China Sea, lower mixing ratios (± standard deviation 1σ) of 1.2 ± 0.3 ppt prevail and also the lowest mixing ratios for $CHBr_3$ during the whole cruise of 0.8 ppt are observed. At the coast of Borneo and the Philippines, the average mixing ratio of $CHBr_3$ increases to 2.3 ± 1.4 ppt. The overall mean $CHBr_3$

mixing ratio during the cruise is 2.1 ± 1.4 ppt (Table 1) and therefore higher than earlier reported $CHBr_3$ observations of 1.2 ppt in January – March 1994 (Yokouchi et al., 1997), 1.1 ppt in September 1994 (Quack and Suess, 1999) and 1.5 ppt in June – July 2009 (Nadzir et al., 2014) further offshore in the South China Sea. The higher atmospheric mixing ratios during the R/V SONNE cruise in November 2011 in contrast to the lower mixing ratios in these previous studies may point to stronger local sources, strong seasonal or interannual variations, or even to long-term changes. CH_2Br_2 shows a mean mixing ratio of 1.2 ± 0.2 ppt (Table 1). Yokouchi et al. (1997) observed a lower mean atmospheric mixing ratio of 0.8 ppt and Nadzir et al. (2014) of 1.0 ppt in the South China Sea. An increase of the CH_2Br_2 mixing ratios from 1.0 ± 0.1 ppt to 1.3 ± 0.2 ppt is observed after November 21, 2011 coinciding with an increase of the CH_3I concentrations from primarily 0.3 ± 0.0 ppt to 0.4 ± 0.1 ppt (Figure 4a). The highest mixing ratio of CH_3I was detected in the southwestern Sulu Sea on November 25, 2011 with 0.8 ppt. The overall mean atmospheric mixing ratio for CH_3I, of 0.4 ± 0.1 ppt (Table 1) is lower than the mean of 0.6 ppt observed by Yokouchi et al. (1997).

The concentration ratio of CH_2Br_2 and $CHBr_3$ (Figure 4b) has been used as an indicator of relative distance to the oceanic source, where a ratio of 0.1 was observed crossing strong coastal source regions (Yokouchi et al., 2005;Carpenter et al., 2003). The ten times elevated $CHBr_3$ has a much shorter lifetime, thus degrading more rapidly than CH_2Br_2, which increases the ratio during transport. Overall, the mean concentration ratio of CH_2Br_2 and $CHBr_3$ is 0.6 ± 0.2, which suggests that predominantly older air masses are advected over the South China Sea.

4.2. Oceanic surface concentrations and emissions from R/V SONNE

VSLS in the surface sea water along the cruise track show highly variable distributions (Figure 4c and Table 1). Oceanic $CHBr_3$ surface concentrations range from 2.8 – 136.9 pmol L^{-1} with a mean of 19.9 pmol L^{-1} during the cruise, while CH_2Br_2 concentrations range from 2.4 – 21.8 pmol L^{-1} with a mean of 5.0 pmol L^{-1}. $CHBr_3$ and CH_2Br_2 have similar distribution patterns in the sampling region with near shore areas showing typically elevated concentrations. CH_3I concentrations range from 0.6 – 18.8 pmol L^{-1} with a mean of 3.8 pmol L^{-1} and show a different distribution along the ship track which might be ascribed to additional photochemical production of CH_3I in the surface waters (e.g. Manley and Dastoor, 1988;Manley and de la Cuesta, 1997;Richter and Wallace, 2004).

High levels of all VSLS are found in waters close to the Malaysian Peninsula, especially in the Singapore Strait on November 16, 2011, possibly showing an anthropogenic influence on

the VSLS concentrations. VSLS concentrations decrease rapidly when the cruise track leads to open ocean waters. Along the west coast (November 19 - 23, 2011) and northeast coast of Borneo (November 25, 2011), bromocarbon concentrations are elevated, and especially $CHBr_3$ concentrations increase in waters with lower salinities, indicating an influence by river run off. Elevated $CHBr_3$ concentrations are often found close to coasts with riverine inputs caused by natural sources and industrial and municipal effluents (see Quack and Wallace, 2003;Fuhlbrügge et al., 2013 and references therein).

Oceanic emissions were calculated from synchronized measurements of sea water concentrations and atmospheric mixing ratios, sea surface temperatures and wind speeds, measured on the ship (Section 2.3.3). The overall VSLS distribution along the ship track is opposite for the oceanic and atmospheric measurements (Figure 4a-d). While the sea water concentrations of VSLS generally decrease towards the Sulu Sea, the atmospheric mixing ratios increase, leading to a generally lower concentration gradient of the compounds between sea water and air in the Sulu Sea (not shown here).

Coinciding low VSLS atmospheric background concentrations, high SSTs, elevated oceanic VSLS concentrations and high wind speeds, lead to high emissions of VSLS for the South China and Sulu Seas (Figure 4d) of 1486 ± 1718 pmol m^{-2} h^{-1} for $CHBr_3$, 405 ± 349 pmol m^{-2} h^{-1} for CH_2Br_2 and 433 ± 482 pmol m^{-2} h^{-1} for CH_3I. In particular, $CHBr_3$ fluxes are very high and thus confirm elevated coastal fluxes from previous campaigns in tropical source regions (Quack et al., 2007). They often exceed 2000 pmol m^{-2} hr^{-1} in the coastal areas and are sometimes higher than 6000 pmol m^{-2} hr^{-1}, as in the Singapore Strait on November 15, 2011 and on November 22, 2011 at the northwest coast of Borneo, which was also an area of strong convection (Figures 1, 4b).

4.3. VSLS intercomparison: R/A FALCON and R/V SONNE

The two profiles of the bromocarbon mixing ratios and the profile for CH_3I from the surface to 13 km altitude as observed on R/A FALCON with the GhOST and WASP instruments (Sala et al., 2014;Tegtmeier et al., 2013) are shown in Figure 5. Mean $CHBr_3$ mixing ratios are 1.43 ppt (GhOST) and 1.90 ppt (WASP) in the MABL (0 – 450 m, determined from meteorological aircraft observations similarly as for the radiosondes, Section 2.2.2) and 0.56 ppt (GhOST) and 1.17 ppt (WASP) in the FT (0.45 km – 13 km, Table 1). The GhOST mixing ratios in the MABL are lower than those observed on R/V SONNE (2.08 ppt). A very good agreement of the measurements is given for the longer lived CH_2Br_2 with 1.17 ppt (R/V SONNE), 1.19 ppt (GhOST) and 1.15 ppt (WASP). CH_3I mixing ratios measured by GhOST

are 0.59 ± 0.30 ppt within the MABL of 450 m height, which is about 0.2 ppt higher than the values from R/V SONNE. Above the MABL, the average mixing ratio of CH_3I decreases to 0.26 ± 0.11 ppt (Figure 5).

$CHBr_3$ and CH_2Br_2 concentrations in the MABL correlate with R = 0.83 for all instruments (Figure 6). $CHBr_3$ and CH_3I concentrations correlate with R = 0.55 and CH_2Br_2 and CH_3I with R = 0.66; all correlations are significant at 99 %. Even higher correlations are found if only measurements on R/V SONNE are taken into account with R = 0.92 for $CHBr_3$ and CH_2Br_2, R = 0.64 for $CHBr_3$ and CH_3I, and R = 0.77 for CH_2Br_2 and CH_3I.

Comparison of R/A FALCON and R/V SONNE data are obtained from their meetings on November, 19 and 21, 2011 (Table 2), when aircraft and ship passed each other within 100 m distance several times, measuring the same air masses. During both meetings, deviations between the GhOST and WASP instruments on the aircraft are larger for the bromocarbons than the deviation between the WASP and the ship measurements. According to Sala et al. (2014) the agreement between the GhOST and WASP instruments are within the expected uncertainty range of both instruments which is then assumed to be also valid for the ship measurements (this study). The good agreement between WASP and ship data might be caused by the same sampling and analysis method, both using stainless steel canisters and subsequent analysis with GC/MS, while GhOST measures in-situ with a different resolution. Since GhOST and WASP measurements together cover a larger spatial area and higher temporal resolution, a mean of both measurements is used in the following for computations in the free troposphere. For CH_3I significantly higher mixing ratios were measured during the meetings between ship and aircraft (Table 2). Whether this offset is systematic for the different methods, needs further investigation.

5. Air mass and VSLS transport from the surface to the free troposphere

5.1. Timescales and intensity of vertical transport

Forward trajectories computed with FLEXPART starting at sea level along the cruise track yield an average MABL residence time of 7.8 ± 3.5 hr before the trajectories enter the FT (Figure 7), reflecting a relatively fast exchange due to the convective well ventilated MABL (Figure 3). The trajectories generally show a strong contribution of surface air masses to the FT, despite some exceptions during November 18 – 22, 2011 (Figure 7). Most intense and rapid transport of MABL air masses up to 13 km height occurs on November 17 and 23, 2011. ~~To estimate the loss of air masses out of the South China Sea area between 5° S – 20°~~

~~N and 100° E – 125° E (Section 2.4.3) we determine the loss of trajectories out of this area after their release (Figure 8). After 4 days, 88 % of all trajectories released along the cruise track are still within this defined area of the South China Sea, and 31 % after 10 days.~~

5.2. Contribution of oceanic emissions to VSLS in the MABL

From the sea – air fluxes (Section 4.2) and the residence times of the surface trajectories in the MABL (Section 5.1), the Oceanic Delivery (OD) and the COnvective Loss (COL) were computed (Table 3) using the method described in Section 2.4.2.

Based on the OD and the COL, the Oceanic Delivery Ratio (ODR) is calculated in order to characterize the relative contribution of the local oceanic emissions compared to the loss of MABL air into the FT (Table 3, Figure 8). The average ODR during the cruise is 0.45 ± 0.55 for $CHBr_3$, which means that the loss from the MABL to the FT is balanced to 45 % by oceanic emissions along the cruise track. The ODR for CH_2Br_2 is 0.20 ± 0.21 and for CH_3I 0.74 ± 1.05, respectively, suggesting that the major amount of CH_3I originates from nearby sources. Similarly to the ODR the CL is related to the COL to derive the Chemical Loss Ratio (CLR) for the VSLS, which is 0.03 ± 0.01 for $CHBr_3$, 0.01 ± 0.00 for CH_2Br_2 and 0.09 ± 0.04 for CH_3I. When compared to the other source and loss processes, the chemical loss appears negligible for all three gases. The ratio of the Advective Delivery (ADR) is 0.58 ± 0.55 for $CHBr_3$, 0.80 ± 0.21 for CH_2Br_2 and 0.35 ± 1.02, implying that most of the observed CH_2Br_2 (80 %) in the MABL is advected from other source regions. Applying the ODR to the observed mixing ratios in the MABL gives an estimate of the VSLS originating from the local oceanic emissions (VMR_{ODR}, Table 4). The local ocean emits a concentration that equates to 0.89 ± 1.12 ppt $CHBr_3$, 0.25 ± 0.26 ppt CH_2Br_2 and 0.28 ± 0.40 ppt CH_3I in the MABL. The average transport from the MABL to the FT ($Flux_{MABL-FT}$), computed from the MABL concentrations and the trajectory residence time in the MABL, is 4240 ± 1889 pmol m^{-2} hr^{-1} for $CHBr_3$, 2419 ± 929 pmol m^{-2} hr^{-1} for CH_2Br_2 and 865 ± 373 pmol m^{-2} hr^{-1} for CH_3I. Calculations with the ERA-Interim MABL height, which is on average 140 m higher than the one derived from the radiosondes, leads to similar estimates (S-Table 1).

Since the wind is a driving factor for oceanic emissions and advection of VSLS, changes in wind speed are assumed to affect atmospheric VSLS mixing ratios in the MABL during this cruise. Significant correlations are found between wind speed and the observed mixing ratios of all three VSLS in the MABL with correlation coefficients of R = 0.55 ($CHBr_3$), R = 0.57 (CH_2Br_2) and R = 0.56 (CH_3I), respectively. Mixing ratios that originate from oceanic

emissions (VMR_{ODR}) correlate significantly to the wind speed with R = 0.52, R = 0.72 and R = 0.62, respectively. On the opposite, VMR_{ADR}, which is calculated as the residual from VMR_{ODR}, is negatively correlated to the wind speed with R = -0.21, R = -0.32 and R = -0.53. The correlations reveal that the contribution of oceanic emissions to MABL VSLS increase for higher wind speeds, while the advective contribution decreases.

5.3. Oceanic contribution to the FT

5.3.1. Identification of VSLS MABL air in the FT

With a simplified approach (method description in Section 2.4.3) we are able to estimate the contribution of MABL air and regional marine sources observed on R/V SONNE to the FT. Individual MABL air masses during the cruise show ~~the strongest~~a strong contribution to the FT air up to 10 % after 10 days~~within the lower 3 km of the atmosphere during the first 6 days after release~~ (Figure 9a-f). The MABL air is rapidly transported into high altitudes before it is dispersed in the FT column. ~~Once the MABL air is spread in the FT column, a decrease of the contribution with time is due to the transport of trajectories out of the predefined South China and Sulu Seas area and their chemical loss (Figure 8).~~

The average contribution of VSLS concentrations in the MABL air to the FT concentrations (C~~ϵ_{MABL}~~) is generally highest for $CHBr_3$, with ~~about 5 – 10~~about 10 – 15 % between 4 – 10 km and up to 25 % above 10 km height~~ % above 3 km height within 10~~ 3 – 10 days after release in the MABL (coloured contours in Figure 9a), followed by CH_2Br_2 (~~2 – 5 %~~5 - 10 % below 10 km and up to 16 % above 10 km height, Figure 9b). The lowest contribution is found for~~r~~ the short-lived CH_3I ~~and only~~with ~~0 – 3~~up to 4 % within 3 days ~~for the short-lived CH_3I~~ (Figure 9c). In general the contribution below 5 km height decreases after about 10 days, when most of the MABL air is transported into higher altitudes. For CH_3I, ~~The~~ the chemical degradation~~ of CH_3I~~, according to its short tropospheric lifetime of 3.5 days, leads to a rapid decrease of the contribution already 3~~2~~ days after release.

To identify the contribution of the oceanic emissions to the FT VSLS during the cruise, the VMR_{ODR} of each compound is used as the initial mixing ratio in the MABL air mass. For $CHBr_3$ and CH_2Br_2 the local emissions contribute only up to ~~6~~11 % and ~~2~~4 % to the FT concentrations (C~~ϵ_{ODR}~~, Figure 9d-e) compared to the 25~~10~~ %, respectively ~~5~~16 %, of ~~ϵ~~C_{MABL}. In contrast, the contribution of the local oceanic emissions of CH_3I (Figure 9f) is almost similar to the contribution of the observed MABL concentrations (Figure 9c).

5.3.2. Accumulated VSLS in the free troposphere

By simulating a steady transport of MABL air masses into the FT, mean accumulated VSLS mixing ratios in the FT along and during the cruise were computed (Figure 10) as described in 2.4.3. The simulated FT mixing ratios of $CHBr_3$ and CH_2Br_2 from the observed MABL (VMR_{MABL}) decrease on average from ~~1.7~~2.1 and 1.~~1~~ 2 ppt at~~ 0.5 km height~~at the surface to 0.6 and ~~0.6~~0.8 ppt at ~~7~~ 3 km height. The simulated $CHBr_3$ mixing ratios are constant up to 8 km height followed by an increase up to 0.9 ppt at 13 km height. Simulated CH_2Br_2 mixing ratios increase between 3 and 11.5 km height up to 1.1 ppt and remain constant above 11.5 km height.~~ and increase again above 8 km up to 0.8 ($CHBr_3$) and 0.8 ppt (CH_2Br_2).~~ Simulated CH_3I shows a decrease from 0.~~20~~ 4 ppt at ~~0.5 km~~the surface to 0.~~05~~ 08 ppt at 3 km. Above this altitude, the simulated mixing ratios of CH_3I are almost constant ~~with 0.05 ppt~~before they slowly increase above 9 km height to 0.10 ppt.

To estimate the accumulated FT mixing ratios solely from oceanic emissions, the VMR_{ODR} is used as the initial MABL mixing ratio (Figure 10). The simulated FT mixing ratios using either VMR_{MABL} or VMR_{ODR} as input reveal a similar vertical pattern, since both simulations are based on the same meteorology and trajectories. While FT mixing ratios based on VMR_{MABL} and VMR_{ODR} are similar for CH_3I and differ by about 0.03 ppt (due to the large oceanic contribution to the MABL mixing ratios), FT mixing ratios from VMR_{ODR} are on average ~0.~~5~~ 4 ppt lower for $CHBr_3$ and ~0.~~6~~ 8 ppt CH_2Br_2 than from VMR_{MABL}. Comparing the simulated VMR_{MABL} FT mixing ratios with the observed FT mixing ratios from R/A FALCON reveals generally stronger vertical variations for the ~~simulations~~ observations in contrast to the ~~observations~~simulations. Still, $CHBr_3$ observations ~~is~~ are well reflected in the ~~overestimated in the~~ VMR_{MABL} simulation between ~~0~~ 2 and ~~4~~ 11 km altitude~~, as well as above 12 km~~. Also the ~~S~~simulated CH_2Br_2 in the FT based on VMR_{MABL} ~~underestimates~~ reflects the ~~observed~~ observations of R/A FALCON ~~mixing ratios between~~very well from the surface up to 9~~ 6 and 10~~ km height. ~~In particular, the maximum between 7 and 9 km height is not reflected in the simulations. However, observations of both bromocarbons are within 1σ of the FT simulations with MABL air.~~ The CH_3I simulations show a distinct underestimation of the observed FT mixing ratios. Adjusting the R/A FALCON values by the identified offset to R/V SONNE (Section 4.3 and Table 2) reveals a better agreement between observed and simulated FT mixing ratios (Figure 10).

5.3.3. Discussion

Oceanic emissions of $CHBr_3$ from the South China Sea contribute on average 45 % to the simulated FT mixing ratios (Figure 11). Simulated FT mixing ratios from MABL observations and observed FT mixing ratios agree quite well up to ~~10~~ 11 km height. Above this altitude the simulated FT mixing ratios, in contrast to the observations increase, which is caused by an overestimation of the convective activity~~outflow~~ in our method. However, despite using this simple approach we are able to simulate mean FT mixing ratios up to 11 km height above the South China Sea in good agreement with observations. Thus, we assume that the observed MABL mixing ratios of $CHBr_3$ and CH_2Br_2 are representative for the South China and Sulu Seas. ~~In case of CH_2Br_2 the underestimation of simulated FT mixing ratios between 6 and 10 km using observed MABL mixing ratios may be due to higher background concentrations of CH_2Br_2 in the mid to upper troposphere given the long atmospheric lifetime of 150 days at these levels.~~

On average, 45 % and 20 % of $CHBr_3$ and CH_2Br_2 abundances~~, respectively,~~ in the MABL, observed on~~by~~ the ship, originate from local oceanic emissions along the ship track. Thus, advection from stronger source regions, possibly along the coast (for $CHBr_3$) and from the West Pacific (CH_2Br_2), are necessary to explain the observed MABL mixing ratios.

In contrast to $CHBr_3$ and CH_2Br_2, the simulated mixing ratios of CH_3I in the FT are strongly underestimated no matter whether observed MABL mixing ratios or oceanic emissions are used. The offset between the simulated and observed FT CH_3I could be caused by additional strong sources of CH_3I in the South China Sea area. Furthermore, modelling or measurement uncertainties may add to this offset.

The simulations use constant atmospheric lifetimes for each compound and neglect lifetime variations with altitude which could impact the simulated abundances. However, the altitude variations of the CH_3I lifetime in the MABL and FT are around 0.5 days (Carpenter et al., 2014) and thus impacts on the simulated abundances are quite small. Therefore, it seems unlikely that the lifetime estimate causes a large underestimation of the FT CH_3I. Additional uncertainties may arise from cloud induced effects on photolysis rates (Tie et al., 2003) and OH levels (e.g. Tie et al., 2003;Rex et al., 2014) impacting the VSLS lifetimes. Deficiencies in the meteorological input fields and the FLEXPART model, in particular in the boundary layer and in the convection parameterizations would affect the transport of all compounds and their contribution to the FT concentrations in a similar way and thus seems to be unlikely as well. Ship and aircraft measurements revealed a possible instrumental offset for CH_3I (Section 4.3). When we adjust the observations for the offset of CH_3I between R/V SONNE and R/A FALCON the simulated and observed FT mixing ratios match better. Thus, an

instrumental offset causing, at least partially, the calculated discrepancy for CH_3I appears likely (Section 2.3.1).

Another explanation for the elevated CH_3I in the FT is advection of fresh air with elevated CH_3I mixing ratios in the FT from e.g. South East Asia or the Philippines. These areas are known to comprise strong sources for atmospheric CH_3I from e.g. rice plantations (Redeker et al., 2003;Lee-Taylor and Redeker, 2005). In combination with convective activity over land, which is common in this area (Hendon and Woodberry, 1993), the high observed FT mixing ratios of CH_3I could be explained, despite the low oceanic contribution during the cruise. The low observed MABL mixing ratios of CH_3I on R/V SONNE may thus also not be representative for the area. Yokouchi et al. (1997) observed higher atmospheric CH_3I mixing ratios in the South China Sea.

Finally, the method of our simplified approach includes uncertainties as well. Different parameterizations for the transfer coefficient k_w such as Liss and Merlivat (1986), which is at the lower end of reported parameterizations, and Wanninkhof and McGillis (1999), which is at the higher end, are discussed in Lennartz et al. (2015). Both lead to a reduction of the oceanic contribution to the atmospheric mixing ratios at the observed average moderate wind speeds (~6 ms^{-1}) when applied to our data. Nonetheless, the general conclusion that local oceanic sources of $CHBr_3$ and CH_3I significantly contribute to MABL mixing ratios remains for the cruise. In times of possible higher wind speeds (>10 ms^{-1}), which are likely for this region, the flux variations between the different parameterizations as well as the oceanic contribution to atmospheric abundances, would increase. Further uncertainties may result from the approach to simulate FT mixing ratios from MABL observations, which does not include e.g. turbulent mixing or entrainment of different air masses containing different VSLS mixing ratios. Since observational studies quantifying the oceanic contribution to atmospheric abundances of VSLS are quite rare, it is difficult to evaluate our findings at the moment and more studies for different oceanic regimes should be carried out to validate our results.

6. Summary

The contribution of oceanic VSLS emissions to marine atmospheric boundary layer (MABL) and free troposphere (FT) air during the SHIVA campaign in November 2011 in the South China and Sulu Seas was investigated in this study. Meteorological parameters were measured near the ocean surface and in the troposphere by regular radiosonde launches on R/V SONNE during the cruise. Oceanic VSLS emissions were determined from simultaneous

atmospheric observations and sea surface water concentrations. The transport from the surface through the MABL into the FT was computed with the trajectory model FLEXPART. The ship campaign was dominated by north-easterly winds with a characteristic moderate mean wind speed of 5.5 ms^{-1}. The radiosonde launches revealed a convective, well-ventilated, weakly developed MABL with an average height of 420 ± 120 m during the cruise. 800,000 forward trajectories, launched from the ocean surface along the cruise track, show a rapid exchange of MABL air with the FT within 7.8 hrs. The observations on R/V SONNE reveal high mean ocean surface concentrations and emissions for $CHBr_3$ (19.94 pmol L^{-1} and 1486 pmol m^{-2} hr^{-1}), CH_2Br_2 (4.99 pmol L^{-1} and 405 pmol m^{-2} hr^{-1}) and CH_3I (3.82 pmol L^{-1} and 433 pmol m^{-2} hr^{-1}) in comparison to other oceanic source regions. Atmospheric mixing ratios in the MABL, on the other hand, are relatively low with mean values of 2.08 ppt $CHBr_3$, 1.17 ppt CH_2Br_2, and 0.39 ppt CH_3I. The contribution of the oceanic VSLS emissions to their MABL concentrations was evaluated by simple source-loss estimates, resulting in an Oceanic Delivery Ratio (ODR). The ODR for $CHBr_3$ is 0.45, revealing that up to 45 % of $CHBr_3$ mixing ratios in the MABL above the marginal seas originated, on average, from local oceanic sources, while 74 % of CH_3I and only 20 % of CH_2Br_2 originates from the local ocean. This indicates that the long-lived CH_2Br_2 is largely advected in the MABL.

We extend our analysis to the FT using VSLS observations from R/A FALCON above the South China Sea. A single MABL air release contributes up to ~~28~~ 25 % ($CHBr_3$), ~~12~~ 16 % (CH_2Br_2) and ~~5~~ 4 % (CH_3I) to the FT mixing ratio (Section 5.3.1). The mean contributions of the local oceanic VSLS to the FT within this MABL air release are up to ~~13~~ 11 % ($CHBr_3$), ~~3~~ 4 % (CH_2Br_2) and 4 % (CH_3I). In order to estimate if the accumulated contributions from the single MABL air releases are sufficient to explain the accumulated VSLS mixing ratios observed in the FT, a steady transport of observed MABL air masses and oceanic emissions into the FT above the South China Sea was simulated. The simulations for $CHBr_3$ based on the volume mixing ratios in the MABL (VMR_{MABL}) reflect the observed mixing ratios in the FT up to 11 km height, while the simulations based on the local oceanic emissions (VMR_{ODR}) explained about ~~60~~ 45 %. In the MABL, the local oceanic emissions along the cruise track also explain half of the $CHBr_3$. Thus, we conclude that the observed mixing ratios of $CHBr_3$ in the MABL are influenced by stronger, possibly coastal sources, in the region.

CH_2Br_2 in the FT, simulated from observed MABL mixing ratios, shows a good agreement between observations and simulations up to 9 km height. ~~However, slightly lower simulated mixing ratios in the mid to upper troposphere compared to the observations indicate an accumulation of CH_2Br_2 at these levels due to its longer atmospheric lifetime compared to~~

~~$CHBr_3$.~~ CH_3I in the FT is underestimated in the simulations, using both the observed MABL mixing ratios and the oceanic emissions. Even addressing an unresolved offset between the ship and aircraft data leads to an underestimation of CH_3I in the FT, which points to additional CH_3I sources, e.g. rice plantations in the region together with pronounced convection.

Our investigations show how oceanic emissions of VSLS in a strong oceanic source region contribute to the observed atmospheric mixing ratios in the MABL. Furthermore, the contributions of these atmospheric mixing ratios, and the local oceanic VSLS, to the observed VSLS in the FT above this source region are derived. The results reveal strong links between oceanic emissions, atmospheric mixing ratios, MABL conditions and prevailing convective activity in the troposphere. The methods should be applied to other oceanic regions to derive a better process understanding of the contributions of air-sea gas exchange on atmospheric abundances. For the detection of future climate change effects on ocean surface trace gas emissions and their influence on atmospheric chemistry and composition it is important to study the complex interplay between oceanic sources and emissions, meteorology, atmospheric mixing ratios, and transport to the upper atmosphere.

Acknowledgements

This work was supported by the EU project SHIVA under grant agreement no. FP7-ENV-2007-1-226224 and by the BMBF grants SHIVA-SONNE 03G0218A and SOPRAN II FKZ 03F0611A. We thank the authorities of Malaysia and the Philippines for the permissions to work in their territorial waters, as well as the SHIVA coordinators Klaus Pfeilsticker and Marcel Dorf and all other SHIVA contributors. We acknowledge the European Centre for medium range weather forecast (ECMWF) for the provision of ERA-Interim reanalysis data and the Lagrangian particle dispersion model FLEXPART used in this publication. We would also like to thank for the support, the captain and crew of R/V SONNE and the pilot in command and crew of R/A FALCON as well as the Projektträger Jülich (PTJ) and the Deutscher Wetterdienst (DWD). E. Atlas was supported by grant #NNX12AH02G from the NASA Upper Atmosphere Research Program. We thank X. Zhu and L. Pope for technical support of canister analysis and C. Marandino for proof reading the manuscript. Additional thanks goes to the Editor M. Schulz for leading the review process and his helpful comments to improve the manuscript, as well as to the two anonymous reviewers.

REFERENCES

Aschmann, J., Sinnhuber, B., Chipperfield, M., and Hossaini, R.: Impact of deep convection and dehydration on bromine loading in the upper troposphere and lower stratosphere, Atmospheric Chemistry and Physics, 11, 2671-2687, 10.5194/acp-11-2671-2011, 2011.

Aschmann, J., and Sinnhuber, B.: Contribution of very short-lived substances to stratospheric bromine loading: uncertainties and constraints, Atmospheric Chemistry and Physics, 13, 1203-1219, 10.5194/acp-13-1203-2013, 2013.

Brinckmann, S., Engel, A., Bonisch, H., Quack, B., and Atlas, E.: Short-lived brominated hydrocarbons - observations in the source regions and the tropical tropopause layer, Atmospheric Chemistry and Physics, 12, 1213-1228, 10.5194/acp-12-1213-2012, 2012.

Carpenter, L., and Liss, P.: On temperate sources of bromoform and other reactive organic bromine gases, Journal of Geophysical Research-Atmospheres, 105, 20539-20547, 10.1029/2000JD900242, 2000.

Carpenter, L., Liss, P., and Penkett, S.: Marine organohalogens in the atmosphere over the Atlantic and Southern Oceans, Journal of Geophysical Research-Atmospheres, 108, 10.1029/2002JD002769, 2003.

Carpenter, L. J., Reimann, S., Burkholder, J. B., Clerbaux, C., Hall, B. D., Hossaini, R., Laube, J. C., and Yvon-Lewis, S. A.: Update on Ozone-Depleting Substances (ODSs) and Other Gases of Interest to the Montreal Protocol, in: Scientific Assessment of Ozone Depletion: 2014, edited by: Engel, A., and Montzka, S. A., World Meteorological Organization, Geneva, 2014.

Dee, D., Uppala, S., Simmons, A., Berrisford, P., Poli, P., Kobayashi, S., Andrae, U., Balmaseda, M., Balsamo, G., Bauer, P., Bechtold, P., Beljaars, A., van de Berg, L., Bidlot, J., Bormann, N., Delsol, C., Dragani, R., Fuentes, M., Geer, A., Haimberger, L., Healy, S., Hersbach, H., Holm, E., Isaksen, L., Kallberg, P., Kohler, M., Matricardi, M., McNally, A., Monge-Sanz, B., Morcrette, J., Park, B., Peubey, C., de Rosnay, P., Tavolato, C., Thepaut, J., and Vitart, F.: The ERA-Interim reanalysis: configuration and performance of the data assimilation system, Quarterly Journal of the Royal Meteorological Society, 137, 553-597, 10.1002/qj.828, 2011.

Dix, B., Baidara, S., Bresch, J., Hall, S., Schmidt, K., Wang, S., and Volkamer, R.: Detection of iodine monoxide in the tropical free troposphere, Proceedings of the National Academy of Sciences of the United States of America, 110, 2035-2040, 10.1073/pnas.1212386110, 2013.

750 Forster, C., Stohl, A., and Seibert, P.: Parameterization of convective transport in a Lagrangian particle
751 dispersion model and its evaluation, Journal of Applied Meteorology and Climatology, 46, 403-422,
752 10.1175/JAM2470.1, 2007.
753 Fuhlbrügge, S., Krüger, K., Quack, B., Atlas, E., Hepach, H., and Ziska, F.: Impact of the marine atmospheric
754 boundary layer conditions on VSLS abundances in the eastern tropical and subtropical North Atlantic Ocean,
755 Atmospheric Chemistry and Physics, 13, 6345-6357, 10.5194/acp-13-6345-2013, 2013.
756 Fuhlbrügge, S., Quack, B., Atlas, E., Fiehn, A., Hepach, H., and Krüger, K.: Meteorological constraints on oceanic
757 halocarbons above the Peruvian Upwelling, Atmos. Chem. Phys. Discuss., 15, 20597–20628, 10.5194/acpd-15-
758 20597-2015, 2015.
759 Gschwend, P., Macfarlane, J., and Newman, K.: Volatile halogenated organic-compounds released to seawater
760 from temperate marine macroalgae, Science, 227, 1033-1035, 10.1126/science.227.4690.1033, 1985.
761 Hendon, H., and Woodberry, K.: The diurnal cycle of tropical convection, Journal of Geophysical Research-
762 Atmospheres, 98, 16623-16637, 10.1029/93JD00525, 1993.
763 Hepach, H., Quack, B., Ziska, F., Fuhlbrügge, S., Atlas, E., Krüger, K., Peeken, I., and Wallace, D. W. R.: Drivers of
764 diel and regional variations of halocarbon emissions from the tropical North East Atlantic, Atmos. Chem. Phys.,
765 14, 10.5194/acp-14-1255-2014, 2014.
766 Hossaini, R., Mantle, H., Chipperfield, M., Montzka, S., Hamer, P., Ziska, E., Quack, B., Kruger, K., Tegtmeier, S.,
767 Atlas, E., Sala, S., Engel, A., Bonisch, H., Keber, T., Oram, D., Mills, G., Ordonez, C., Saiz-Lopez, A., Warwick, N.,
768 Liang, Q., Feng, W., Moore, E., Miller, B., Marecal, V., Richards, N., Dorf, M., and Pfeilsticker, K.: Evaluating
769 global emission inventories of biogenic bromocarbons, Atmospheric Chemistry and Physics, 13, 11819-11838,
770 10.5194/acp-13-11819-2013, 2013.
771 Hossaini, R., Chipperfield, M., Montzka, S., Rap, A., Dhomse, S., and Feng, W.: Efficiency of short-lived halogens
772 at influencing climate through depletion of stratospheric ozone, Nature Geoscience, 8, 186-190,
773 10.1038/NGEO2363, 2015.
774 Hughes, C., Johnson, M., von Glasow, R., Chance, R., Atkinson, H., Souster, T., Lee, G., Clarke, A., Meredith, M.,
775 Venables, H., Turner, S., Malin, G., and Liss, P.: Climate-induced change in biogenic bromine emissions from
776 the Antarctic marine biosphere, Global Biogeochemical Cycles, 26, 10.1029/2012GB004295, 2012.
777 Krüger, K., and Quack, B.: Introduction to special issue: the TransBrom Sonne expedition in the tropical West
778 Pacific, Atmospheric Chemistry and Physics, 13, 9439-9446, 10.5194/acp-13-9439-2013, 2013.
779 Lee-Taylor, J., and Redeker, K.: Reevaluation of global emissions from rice paddies of methyl iodide and other
780 species, Geophysical Research Letters, 32, 10.1029/2005GL022918, 2005.
781 Leedham, E., Hughes, C., Keng, F., Phang, S., Malin, G., and Sturges, W.: Emission of atmospherically significant
782 halocarbons by naturally occurring and farmed tropical macroalgae, Biogeosciences, 10, 3615-3633,
783 10.5194/bg-10-3615-2013, 2013.
784 Lennartz, S. T., Krysztofiak, G., Marandino, C. A., Sinnhuber, B. M., Tegtmeier, S., Ziska, F., Hossaini, R., Krüger,
785 K., Montzka, S. A., Atlas, E., Oram, D. E., Keber, T., Bönisch, H., and Quack, B.: Modelling marine emissions and
786 atmospheric distributions of halocarbons and dimethyl sulfide: the influence of prescribed water
787 concentration vs. prescribed emissions, Atmos. Chem. Phys., 15, 11753-11772, 10.5194/acp-15-11753-2015,
788 2015.
789 Liss, P. S., and Merlivat, L.: Air-Sea Gas Exchange Rates: Introduction and Synthesis, in: The Role of Air-Sea
790 Exchange in Geochemical Cycling, edited by: Buat-Menard, P., Reidel, D., and Norwell, M., Springer
791 Netherlands, 113-127, 1986.
792 Liu, Y., Yvon-Lewis, S., Thornton, D., Butler, J., Bianchi, T., Campbell, L., Hu, L., and Smith, R.: Spatial and
793 temporal distributions of bromoform and dibromomethane in the Atlantic Ocean and their relationship with
794 photosynthetic biomass, Journal of Geophysical Research-Oceans, 118, 3950-3965, 10.1002/jgrc.20299, 2013.
795 Manley, S., and Dastoor, M.: Methyl-iodide (CH3I) production by kelp and assoviated microbes, Marine
796 Biology, 98, 477-482, 10.1007/BF00391538, 1988.
797 Manley, S. L., and de la Cuesta, J. L.: Methyl iodide production from marine phytoplankton cultures, Limnology
798 and Oceanography, 42, 142-147, 1997.
799 Montzka, S., Butler, J., Hall, B., Mondeel, D., and Elkins, J.: A decline in tropospheric organic bromine,
800 Geophysical Research Letters, 30, 10.1029/2003GL017745, 2003.
801 Montzka, S. A., and Reimann, S.: Ozone-depleting substances and related chemicals, Scientific Assessment of
802 Ozone Depletion: 2010, Global Ozone Research and Monitoring Project – Report No. 52, Geneva, Switzerland,
803 2011.
804 Nadzir, M., Phang, S., Abas, M., Rahman, N., Abu Samah, A., Sturges, W., Oram, D., Mills, G., Leedham, E., Pyle,
805 J., Harris, N., Robinson, A., Ashfold, M., Mead, M., Latif, M., Khan, M., Amiruddin, A., Banan, N., and Hanafiah,
806 M.: Bromocarbons in the tropical coastal and open ocean atmosphere during the 2009 Prime Expedition

807 Scientific Cruise (PESC-09), Atmospheric Chemistry and Physics, 14, 8137-8148, 10.5194/acp-14-8137-2014,
808 2014.
809 Nightingale, P., Malin, G., Law, C., Watson, A., Liss, P., Liddicoat, M., Boutin, J., and Upstill-Goddard, R.: In situ
810 evaluation of air-sea gas exchange parameterizations using novel conservative and volatile tracers, Global
811 Biogeochemical Cycles, 14, 373-387, 10.1029/1999GB900091, 2000.
812 Quack, B., and Suess, E.: Volatile halogenated hydrocarbons over the western Pacific between 43 degrees and
813 4 degrees N, Journal of Geophysical Research-Atmospheres, 104, 1663-1678, 10.1029/98JD02730, 1999.
814 Quack, B., and Wallace, D.: Air-sea flux of bromoform: Controls, rates, and implications, Global Biogeochemical
815 Cycles, 17, 10.1029/2002GB001890, 2003.
816 Quack, B., Atlas, E., Petrick, G., and Wallace, D.: Bromoform and dibromomethane above the Mauritanian
817 upwelling: Atmospheric distributions and oceanic emissions, Journal of Geophysical Research-Atmospheres,
818 112, 10.1029/2006JD007614, 2007.
819 Quack, B., Krüger, K., Atlas, E., Tegtmeier, S., Großmann, K., Rex, M., von Glasow, R., Sommariva, R., and
820 Wallace, D.: Halocarbon sources and emissions over the Western Pacific, oral presentation on 05.04.2011,
821 EGU, Vienna, Austria, 2011.
822 Redeker, K., Meinardi, S., Blake, D., and Sass, R.: Gaseous emissions from flooded rice paddy agriculture,
823 Journal of Geophysical Research-Atmospheres, 108, 10.1029/2002JD002814, 2003.
824 Rex, M., Wohltmann, I., Ridder, T., Lehmann, R., Rosenlof, K., Wennberg, P., Weisenstein, D., Notholt, J.,
825 Kruger, K., Mohr, V., and Tegtmeier, S.: A tropical West Pacific OH minimum and implications for stratospheric
826 composition, Atmospheric Chemistry and Physics, 14, 4827-4841, 10.5194/acp-14-4827-2014, 2014.
827 Richter, U., and Wallace, D.: Production of methyl iodide in the tropical Atlantic Ocean, Geophysical Research
828 Letters, 31, 10.1029/2004GL020779, 2004.
829 Saiz-Lopez, A., and von Glasow, R.: Reactive halogen chemistry in the troposphere, Chemical Society Reviews,
830 41, 6448-6472, 10.1039/c2cs35208g, 2012.
831 Saiz-Lopez, A., Fernandez, R., Ordonez, C., Kinnison, D., Martin, J., Lamarque, J., and Tilmes, S.: Iodine
832 chemistry in the troposphere and its effect on ozone, Atmospheric Chemistry and Physics, 14, 13119-13143,
833 10.5194/acp-14-13119-2014, 2014.
834 Sala, S., Bonisch, H., Keber, T., Oram, D., Mills, G., and Engel, A.: Deriving an atmospheric budget of total
835 organic bromine using airborne in situ measurements from the western Pacific area during SHIVA,
836 Atmospheric Chemistry and Physics, 14, 6903-6923, 10.5194/acp-14-6903-2014, 2014.
837 Schauffler, S., Atlas, E., Blake, D., Flocke, F., Lueb, R., Lee-Taylor, J., Stroud, V., and Travnicek, W.: Distributions
838 of brominated organic compounds in the troposphere and lower stratosphere, Journal of Geophysical
839 Research-Atmospheres, 104, 21513-21535, 10.1029/1999JD900197, 1999.
840 Seibert, P., Beyrich, F., Gryning, S., Joffre, S., Rasmussen, A., and Tercier, P.: Review and intercomparison of
841 operational methods for the determination of the mixing height, Atmospheric Environment, 34, 1001-1027,
842 10.1016/S1352-2310(99)00349-0, 2000.
843 Solomon, S.: Stratospheric ozone depletion: A review of concepts and history, Reviews of Geophysics, 37, 275-
844 316, 10.1029/1999RG900008, 1999.
845 Sorensen, J.: Sensitivity of the DERMA long-range gaussian dispersion model to meteorological input and
846 diffusion parameters, Atmospheric Environment, 32, 4195-4206, 10.1016/S1352-2310(98)00178-2, 1998.
847 Stohl, A., Hittenberger, M., and Wotawa, G.: Validation of the Lagrangian particle dispersion model FLEXPART
848 against large-scale tracer experiment data, Atmospheric Environment, 32, 4245-4264, 10.1016/S1352-
849 2310(98)00184-8, 1998.
850 Stohl, A., and Thomson, D.: A density correction for Lagrangian particle dispersion models, Boundary-Layer
851 Meteorology, 90, 155-167, 10.1023/A:1001741110696, 1999.
852 Stohl, A., and Trickl, T.: A textbook example of long-range transport: Simultaneous observation of ozone
853 maxima of stratospheric and North American origin in the free troposphere over Europe, Journal of
854 Geophysical Research-Atmospheres, 104, 30445-30462, 10.1029/1999JD900803, 1999.
855 Stohl, A., Forster, C., Frank, A., Seibert, P., and Wotawa, G.: Technical note: The Lagrangian particle dispersion
856 model FLEXPART version 6.2, Atmospheric Chemistry and Physics, 5, 2461-2474, 2005.
857 Stull, R.: An Introduction to Boundary Layer Meteorology, Kluwer Academic Publishers, Dordrecht, 1988.
858 Tegtmeier, S., Krüger, K., Quack, B., Atlas, E. L., Pisso, I., Stohl, A., and Yang, X.: Emission and transport of
859 bromocarbons: from the West Pacific ocean into the stratosphere, Atmos. Chem. Phys., 12, 10633-10648,
860 10.5194/acp-12-10633-2012, 2012.
861 Tegtmeier, S., Kruger, K., Quack, B., Atlas, E., Blake, D., Boenisch, H., Engel, A., Hepach, H., Hossaini, R.,
862 Navarro, M., Raimund, S., Sala, S., Shi, Q., and Ziska, E.: The contribution of oceanic methyl iodide to

stratospheric iodine, Atmospheric Chemistry and Physics, 13, 11869-11886, 10.5194/acp-13-11869-2013, 2013.
Tie, X., Madronich, S., Walters, S., Zhang, R., Rasch, P., and Collins, W.: Effect of clouds on photolysis and oxidants in the troposphere, Journal of Geophysical Research-Atmospheres, 108, 10.1029/2003JD003659, 2003.
Troen, I., and Mahrt, L.: A simple-model of the atmospheric boundary-layer: Sensitivity to surface evaporation, Boundary-Layer Meteorology, 37, 129-148, 10.1007/BF00122760, 1986.
Vogelezang, D., and Holtslag, A.: Evaluation and model impacts of alternative boundary-layer height formulations, Boundary-Layer Meteorology, 81, 245-269, 10.1007/BF02430331, 1996.
von Glasow, R., von Kuhlmann, R., Lawrence, M., Platt, U., and Crutzen, P.: Impact of reactive bromine chemistry in the troposphere, Atmospheric Chemistry and Physics, 4, 2481-2497, 2004.
Wanninkhof, R., and McGillis, W.: A cubic relationship between air-sea CO2 exchange and wind speed, Geophysical Research Letters, 26, 1889-1892, 10.1029/1999GL900363, 1999.
Worton, D., Mills, G., Oram, D., and Sturges, W.: Gas chromatography negative ion chemical ionization mass spectrometry: Application to the detection of alkyl nitrates and halocarbons in the atmosphere, Journal of Chromatography a, 1201, 112-119, 10.1016/j.chroma.2008.06.019, 2008.
Yang, X., Cox, R., Warwick, N., Pyle, J., Carver, G., O'Connor, F., and Savage, N.: Tropospheric bromine chemistry and its impacts on ozone: A model study, Journal of Geophysical Research-Atmospheres, 110, 10.1029/2005JD006244, 2005.
Yang, X., Abraham, N., Archibald, A., Braesicke, P., Keeble, J., Telford, P., Warwick, N., and Pyle, J.: How sensitive is the recovery of stratospheric ozone to changes in concentrations of very short-lived bromocarbons?, Atmospheric Chemistry and Physics, 14, 10431-10438, 10.5194/acp-14-10431-2014, 2014.
Yokouchi, Y., Mukai, H., Yamamoto, H., Otsuki, A., Saitoh, C., and Nojiri, Y.: Distribution of methyl iodide, ethyl iodide, bromoform, and dibromomethane over the ocean (east and southeast Asian seas and the western Pacific), Journal of Geophysical Research-Atmospheres, 102, 8805-8809, 10.1029/96JD03384, 1997.
Yokouchi, Y., Hasebe, F., Fujiwara, M., Takashima, H., Shiotani, M., Nishi, N., Kanaya, Y., Hashimoto, S., Fraser, P., Toom-Sauntry, D., Mukai, H., and Nojiri, Y.: Correlations and emission ratios among bromoform, dibromochloromethane, and dibromomethane in the atmosphere, Journal of Geophysical Research-Atmospheres, 110, 10.1029/2005JD006303, 2005.
Ziska, F., Quack, B., Abrahamsson, K., Archer, S., Atlas, E., Bell, T., Butler, J., Carpenter, L., Jones, C., Harris, N., Hepach, H., Heumann, K., Hughes, C., Kuss, J., Kruger, K., Liss, P., Moore, R., Orlikowska, A., Raimund, S., Reeves, C., Reifenhauser, W., Robinson, A., Schall, C., Tanhua, T., Tegtmeier, S., Turner, S., Wang, L., Wallace, D., Williams, J., Yamamoto, H., Yvon-Lewis, S., and Yokouchi, Y.: Global sea-to-air flux climatology for bromoform, dibromomethane and methyl iodide, Atmospheric Chemistry and Physics, 13, 8915-8934, 10.5194/acp-13-8915-2013, 2013.

Figures

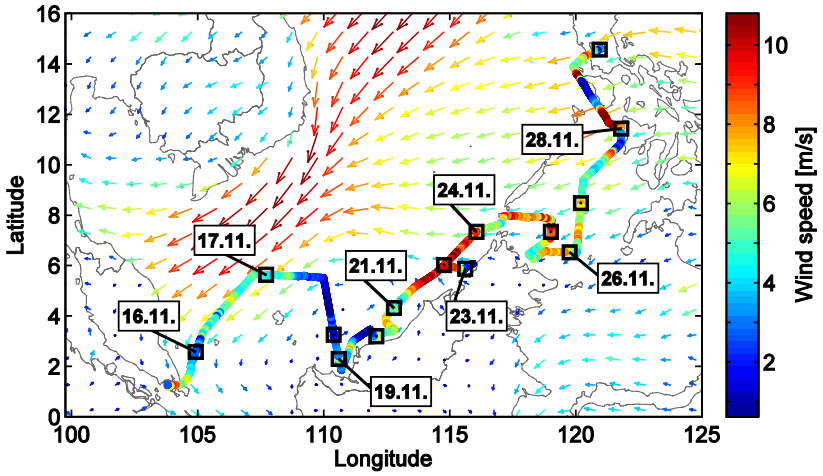

Figure 1: ERA-Interim mean wind field November 15 – 30, 2011 (arrows) and 10 minute running mean of wind speed observed on R/V SONNE as the cruise track. The black squares show the ships position at 00 UTC each day.

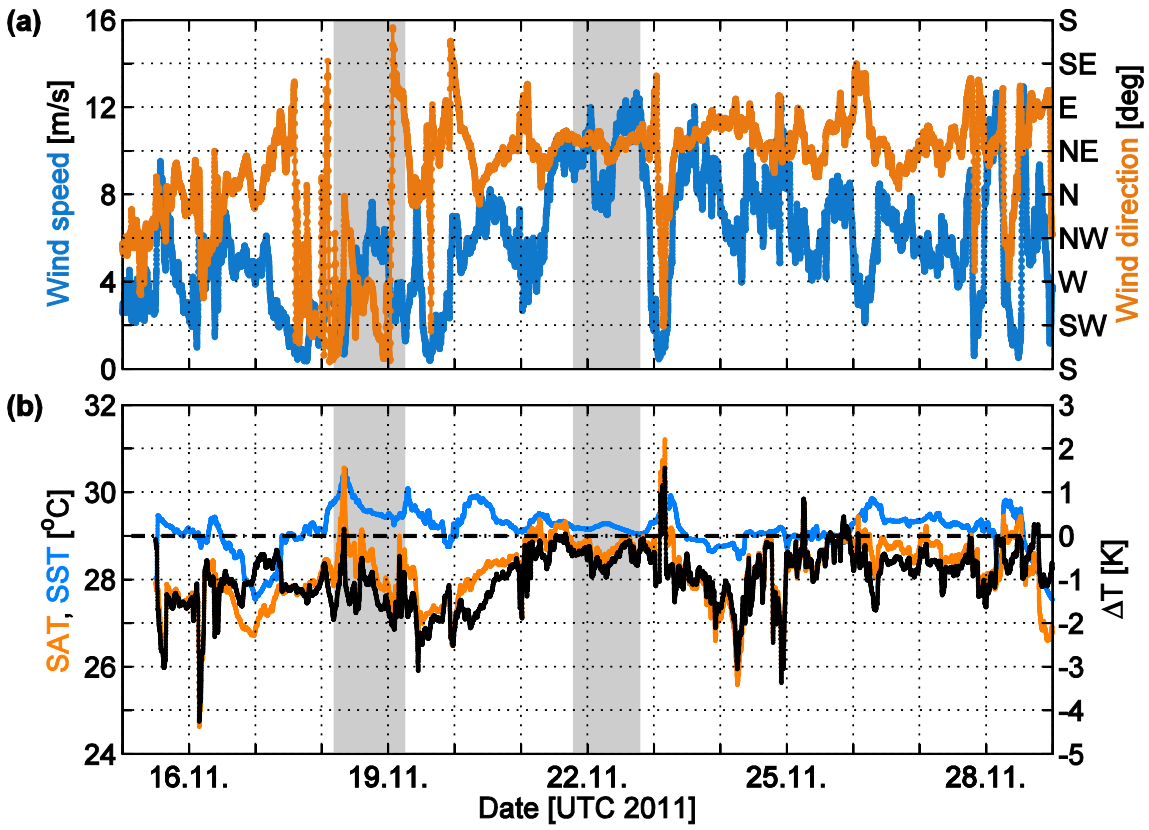

905

906 Figure 2 a-b: Time series of (a) wind speed (blue) and wind direction (orange) and (b) surface
907 air temperature (SAT, orange) and sea surface temperature (SST, blue) on the left scale, as
908 observed on R/V SONNE. The temperature difference of SAT and SST (ΔT) is given on the
909 right scale in (b). The~~A~~ ΔT of 0 K is drawn~~given~~ by a dashed line. The shaded areas (grey) in
910 the background show the 24 h stations. The data are averaged by a 10-minute running mean.

911

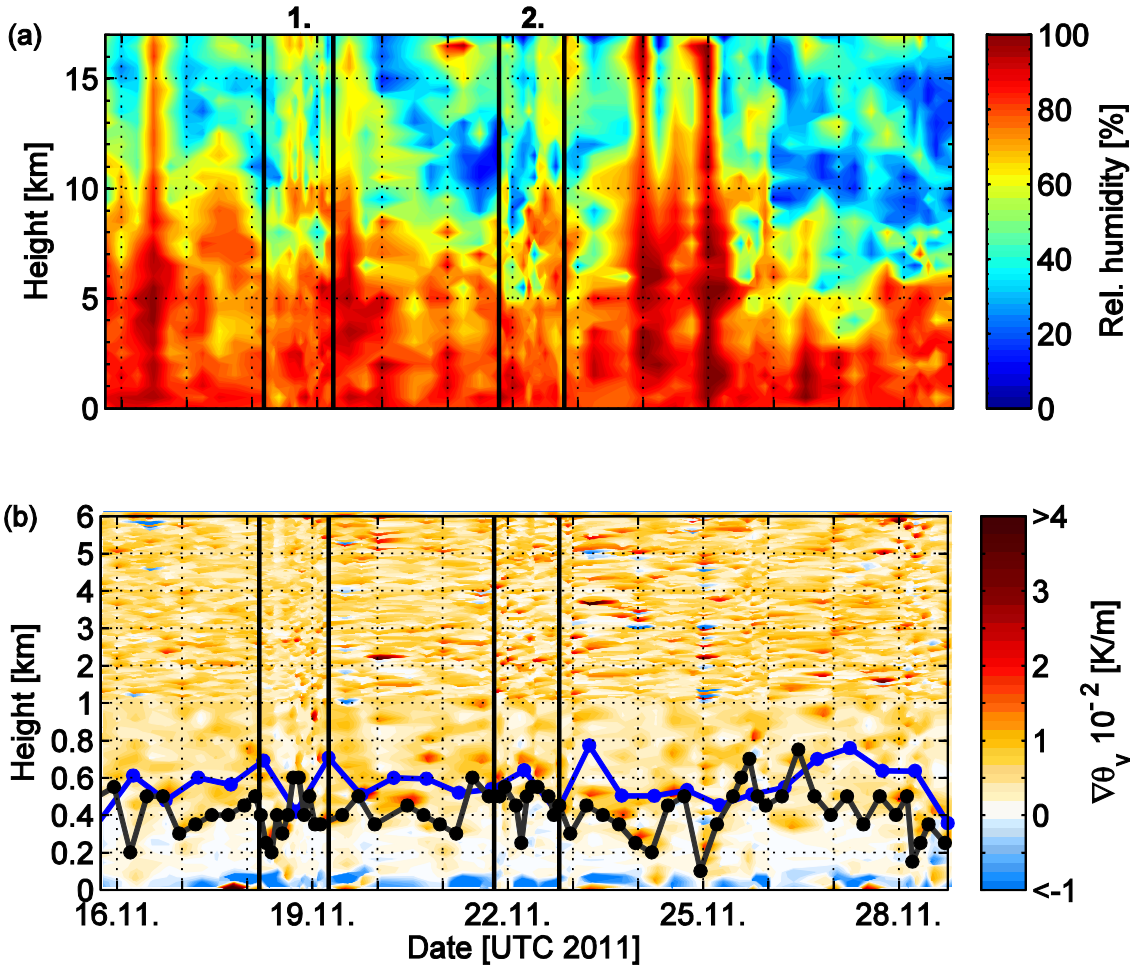

912

913

914 Figure 3: (a) Relative humidity from~~by~~ radiosondes up to 17 km height, the mean cold point
915 tropopause level. The dashed lines and the two numbers above the figure indicate the two 24
916 h stations. (b) Virtual potential temperature gradient as indicator for atmospheric stability
917 (red for stable, white for neutral and blue for unstable) with MABL height derived from
918 radiosondes (black curve) and from ERA-Interim (blue curve). The y-axis is non-linear. The
919 lower 1 km is enlarged to display the stability around the MABL height. The vertical lines
920 and the two numbers above the figures indicate the two 24 h stations.

921

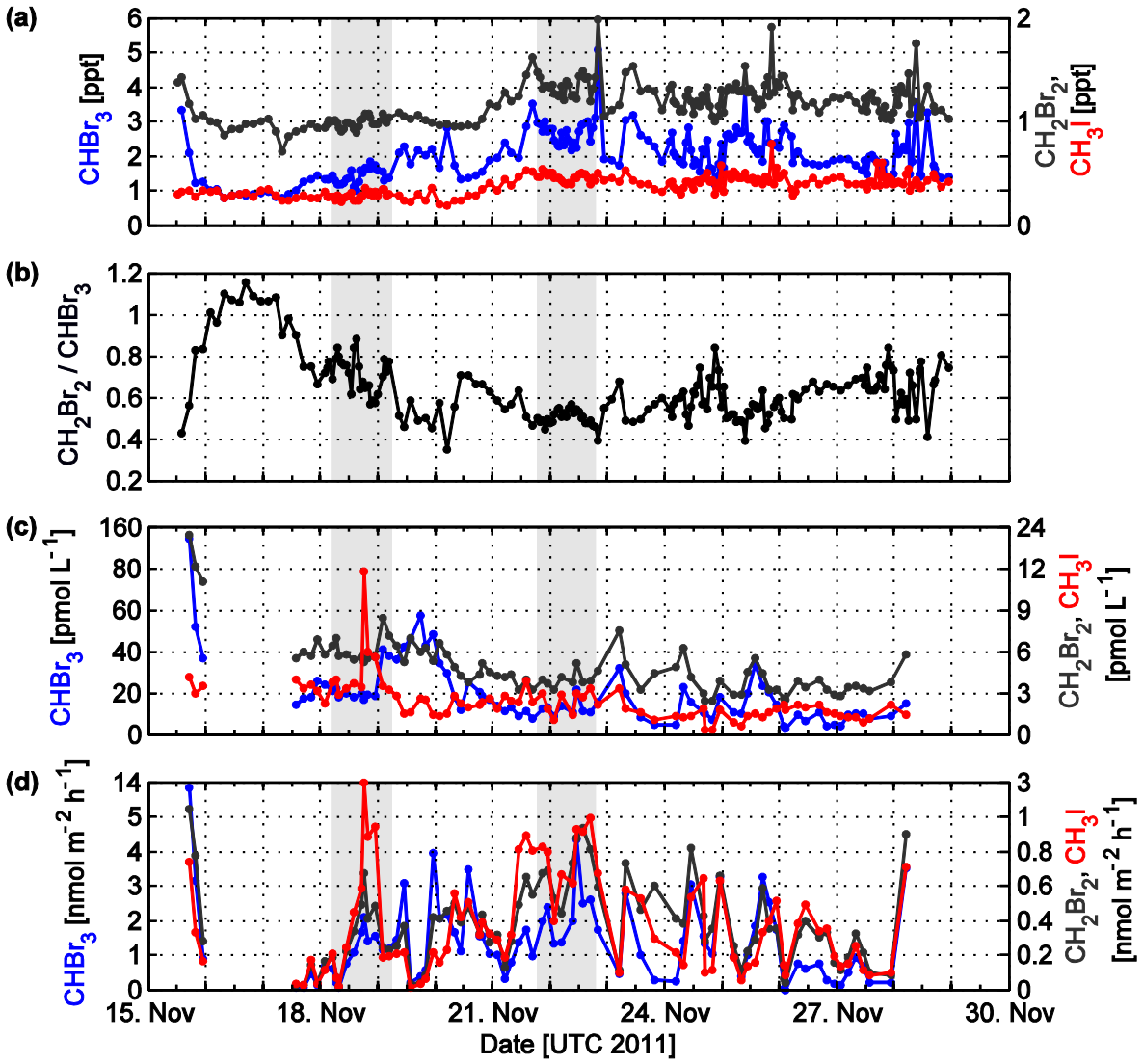

Figure 4 a-d: (a) Atmospheric mixing ratios of $CHBr_3$ (blue), CH_2Br_2 (dark grey) and CH_3I (red) measured on R/V SONNE. (b) Concentration ratio of CH_2Br_2 and $CHBr_3$ on R/V SONNE. (c) Water concentrations of CH_3I, $CHBr_3$ and CH_2Br_2 measured on R/V SONNE. (d) Calculated emissions of $CHBr_3$, CH_2Br_2 and CH_3I from atmospheric and water samples measured on R/V SONNE. The two shaded areas (light grey) in the background show the 24 h stations. Y-axis for (c) and (d) are non-linear.

Table 1: Mean ± standard deviation and range of atmospheric mixing ratios observed on R/V SONNE (195 data points) and R/A FALCON (GhOST-MS with 513 and WASP GC/MS with 202 data points) in the MABL and the FT, water concentrations observed on R/V SONNE and the computed sea – air fluxes. MABL and FT mixing ratios on R/A FALCON are adopted from Sala et al. (2014) and Tegtmeier et al. (2013). The R/A FALCON MABL height was analysed to be 450 m (Sala et al., 2014).

				$CHBr_3$	CH_2Br_2	CH_3I
Atmosph. mixing ratios [ppt]	R/V SONNE			2.08 ± 1.36 [0.79 – 5.07]	1.17 ± 0.19 [0.71 - 1.98]	0.39 ± 0.09 [0.19 – 0.78]
	R/A FALCON	GhOST	MABL	1.43 ± 0.53 [0.42 – 3.42]	1.19 ± 0.21 [0.58 – 1.89]	0. 59 ± 0.30 [0.29 - 3.23]
			FT	0.56 ± 0.17 [0.16 – 2.15]	0.87 ± 0.12 [0.56 – 1.54]	0.26 ± 0.11 [0.08 – 0.80]
		WASP	MABL	1.90 ± 0.55 [0.99 – 3.78]	1.15 ± 0.14 [0.85 – 1.59]	/
			FT	1.17 ± 0.50 [0.43 – 3.22]	0.88 ± 0.14 [0.46 – 1.36]	/
Water concentrations [pmol L^{-1}]				19.94 ± 17.90 [2.80 – 136.91]	4.99 ± 2.59 [2.43 – 21.82]	3.82 ± 2.43 [0.55 – 18.84]
Sea – air flux [pmol m^{-2} h^{-1}]				1486 ± 1718 [-8 – 13149]	405 ± 349 [16 - 2210]	433 ± 482 [13 - 2980]

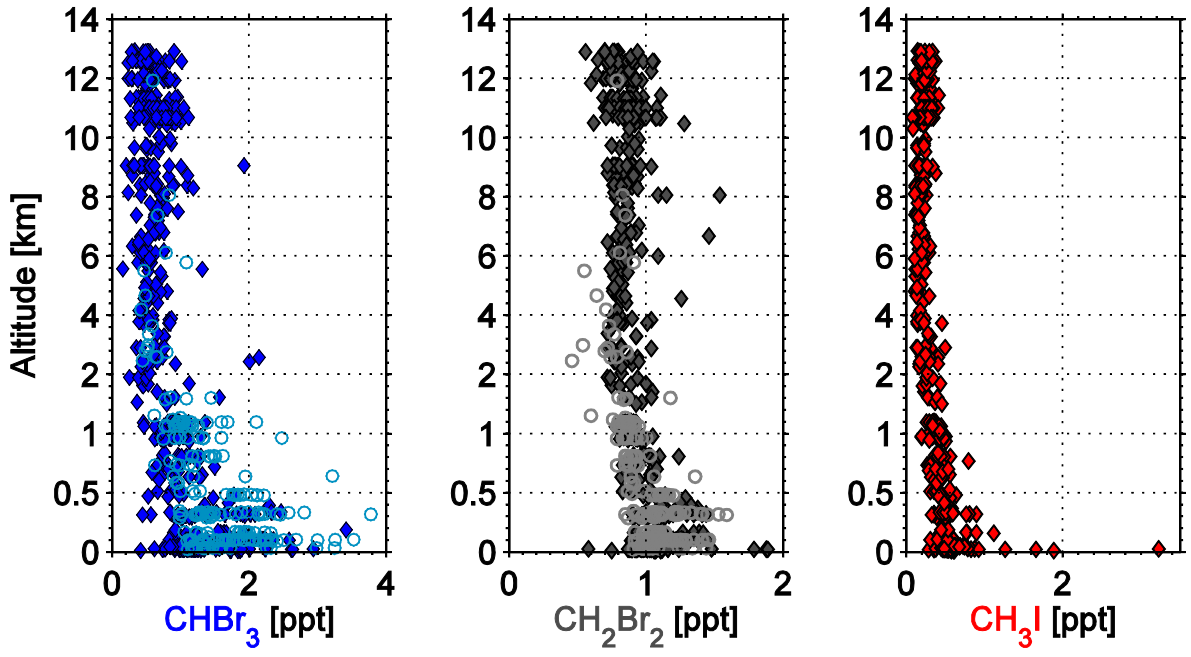

Figure 5: Vertical distribution $CHBr_3$ (blue), CH_2Br_2 (grey) and CH_3I (red) mixing ratios measured in-situ by GhOST (diamonds) and with flasks by WASP (circles) on R/A FALCON. CH_3I was only measured in-situ by GhOST. The lower 2 km are non-linear displayed.

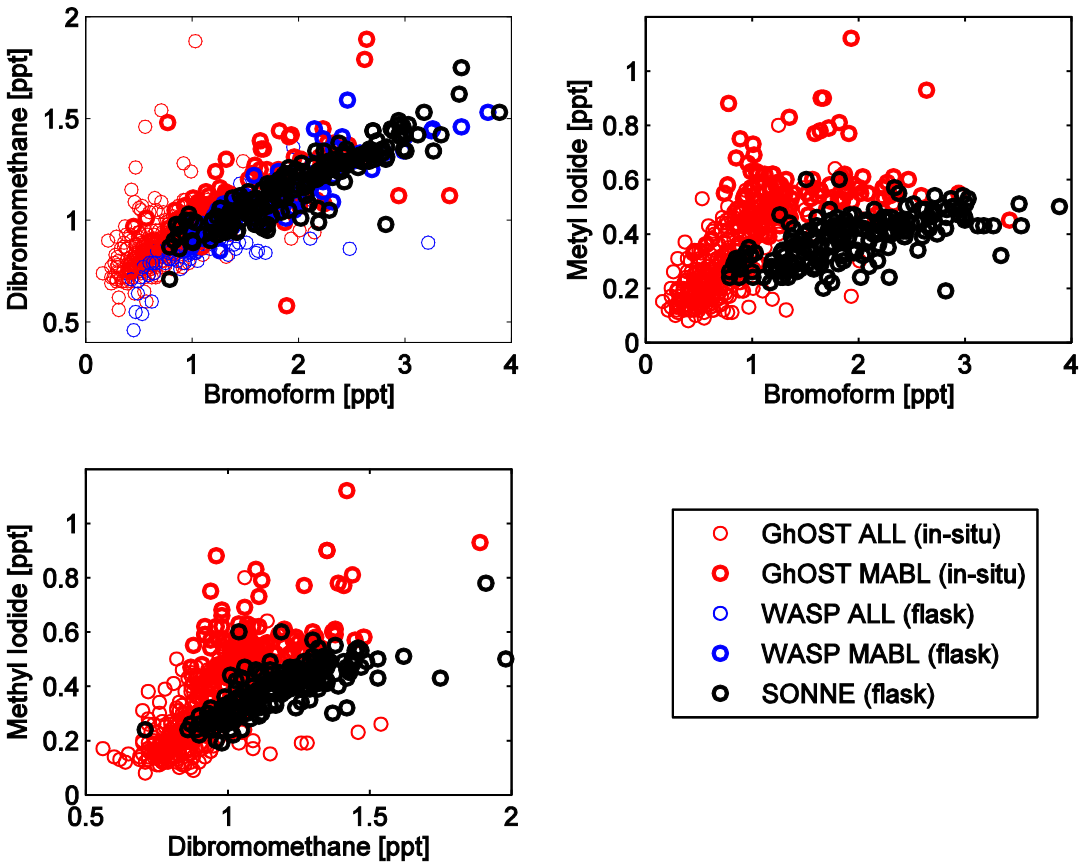

942

943 Figure 6: Correlation of bromoform and CH_2Br_2 (upper left), bromoform and CH_3I (upper
944 right), and CH_2Br_2 and CH_3I (lower left) from GhOST and WASP for all heights (ALL) and
945 only within the MABL (MABL) and from R/V SONNE.

Table 2: Mean atmospheric mixing ratios of $CHBr_3$, CH_2Br_2 and CH_3I observed on R/V SONNE and R/A FALCON during two case studies on 19.11.2011 at 3.2° N and 112.5° E and on 21.11.2011 at 4.6° N and 113.0° E. During the two meetings two (one) measurements have been taken by R/V SONNE, 20 (5) measurements on R/A FALCON by GhOST and 17 (21) by WASP.

		$CHBr_3$ [ppt]	CH_2Br_2 [ppt]	CH_3I [ppt]
November 19, 2011	R/V SONNE	1.37	0.99	0.29
	R/A FALCON: GhOST / WASP	1.02 / 1.37	0.94 / 1.03	0.45 / -
November 21, 2011	R/V SONNE	2.05	1.08	0.28
	R/A FALCON: GhOST / WASP	1.63 / 2.00	1.31 / 1.08	0.82 / -

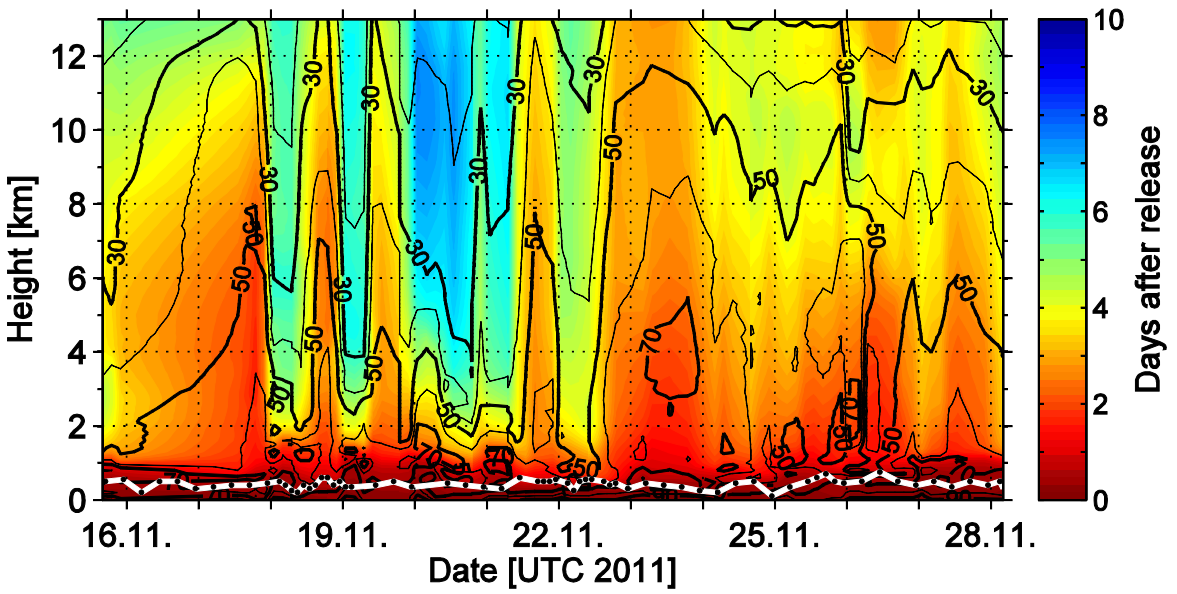

953

954 Figure 7: Forward trajectory runs along the cruise track with FLEXPART using ERA-Interim
955 data. The black contour lines show the mean amount of trajectories (in %) reaching this
956 height within the specific time (colour shading). The white line indicates the radiosonde
957 MABL height.

958

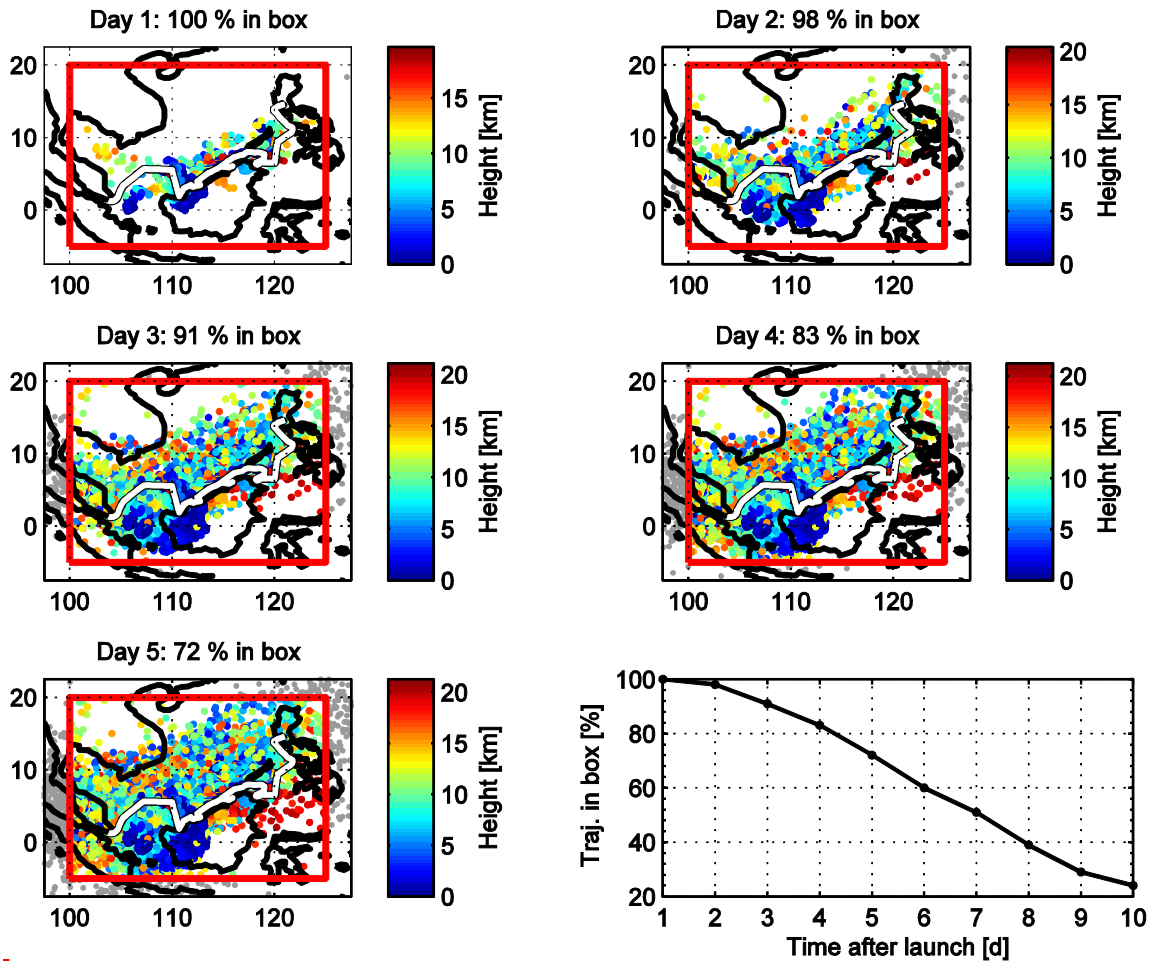

Figure 8: Horizontal distribution, altitude and amount of trajectories over time during the cruise. The red box represents the South China and Sulu Seas area. The lower right plot shows the amount of trajectories that remain in the box with time from all trajectory releases.

Table 3: Mean ± standard deviation of Oceanic Delivery (OD), COnvective Loss (COL), Chemical Loss (CL), Advective Delivery (AD), Oceanic Delivery Ratio (ODR), Chemical Loss Ratio (CLR), and Advective Delivery Ratio (ADR) for $CHBr_3$, CH_2Br_2 and CH_3I.

	OD [% d^{-1}]	COL [% d^{-1}]	CL [% d^{-1}]	AD [% d^{-1}]	ODR	CLR	ADR
$CHBr_3$	116.4 ± 163.6	-307.6 ± 124.3	-7.1	198.2 ± 199.7	0.45 ± 0.55	-0.03 ± 0.01	0.58 ± 0.55
CH_2Br_2	54.2 ± 66.7	-307.6 ± 124.3	-1.2	254.6 ± 131.9	0.20 ± 0.21	-0.00 ± 0.00	0.80 ± 0.21
CH_3I	166.5 ± 185.8	-307.6 ± 124.3	-24.0	165.2 ± 242.3	0.74 ± 1.05	-0.09 ± 0.04	0.35 ± 1.02

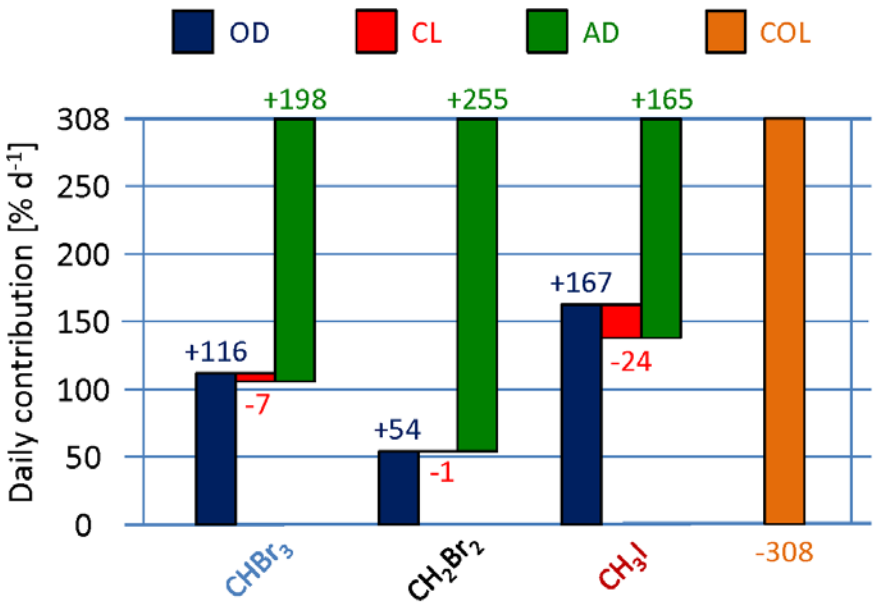

969

970 Figure 8: Average budgets of the Oceanic Delivery (OD, blue), Chemical Loss (CL, red),
971 Advective Delivery (AD, green) and Convective Loss (COL, orange) of $CHBr_3$, CH_2Br_2 and
972 CH_3I in the Marine Atmospheric Boundary Layer (MABL).

973

Table 4: Mean ± standard deviation of observed ~~Volume Mixing Ratios~~mixing ratios in the MABL on R/V SONNE (VMR_{MABL}) versus the amount of VMR originating from oceanic emissions (VMR_{ODR}), chemically degraded according to the specific lifetime (VMR_{CLR}), originating from advection (VMR_{ADR}) and the Flux from the MABL into the FT ($Flux_{MABL-FT}$) for $CHBr_3$, CH_2Br_2 and CH_3I.

	VMR_{MABL} [ppt]	VMR_{ODR} [ppt]	VMR_{CLR} [ppt]	VMR_{ADR} [ppt]	$Flux_{MABL-FT}$ [pmol m^{-2} hr^{1}]
$CHBr_3$	2.08 ± 1.36	0.89 ± 1.12	-0.06 ± 0.04	1.18 ± 1.20	4240 ± 1889
CH_2Br_2	1.17 ± 0.19	0.25 ± 0.26	-0.01 ± 0.00	0.92 ± 0.27	2419 ± 929
CH_3I	0.39 ± 0.09	0.28 ± 0.40	-0.04 ± 0.02	0.13 ± 0.37	865 ± 373

Table 5: Correlation coefficients between wind speed and VSLS MABL mixing ratios (VMR_{MABL}), the Oceanic Delivery (OD), the COnvective Loss to the FT (COL), the Advective Delivery (AD), computed as the residual of OD, and the mixing ratios originating from the OD (VMR_{ODR}) and from the AD (VMR_{ADR}) of each compound. Bold numbers are significant at the 95 % level (p-value).

Wind speed	$CHBr_3$	CH_2Br_2	CH_3I
VMR_{MABL}	**0.55**	**0.57**	**0.56**
OD	**0.31**	**0.48**	**0.52**
COL		**-0.33**	
AD	-0.46	0.56	**-0.57**
VMR_{ODR}	**0.52**	**0.72**	**0.62**
VMR_{ADR}	-0.17	**-0.31**	**-0.49**

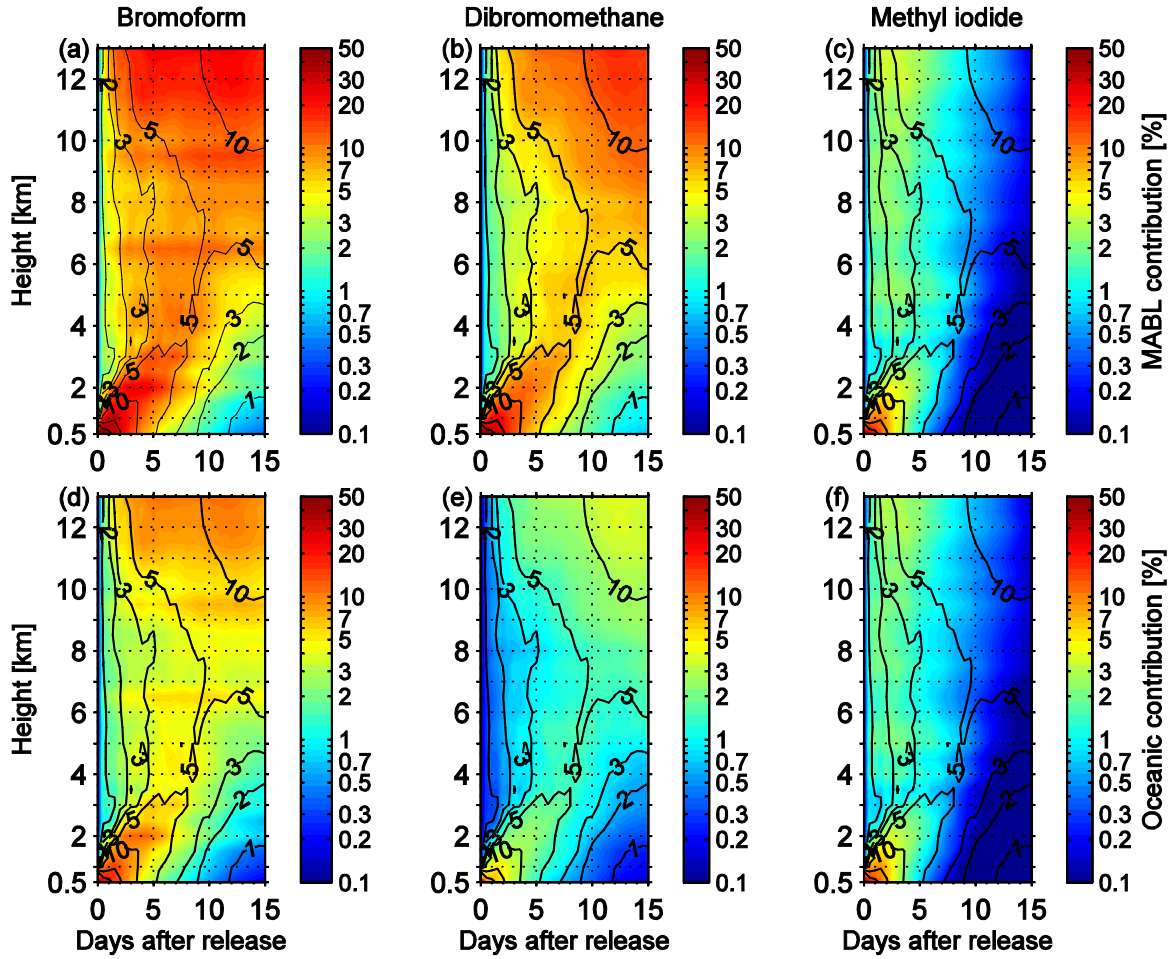

Figure 9: Mean MABL air contribution (a – c) and oceanic contribution (d – f) to observed FT mixing ratios observed by R/A FALCON for three VSLS. The black contour lines show the mean portion of MABL air masses in the FT [%], the colours show the oceanic contribution to the observed compounds in the FT at specific height and day after release [%] including chemical degradation~~, the loss out of the South China Sea area with time~~ and the vertical density driven extension of MABL air masses. The scale of the coloured contour is logarithmic.

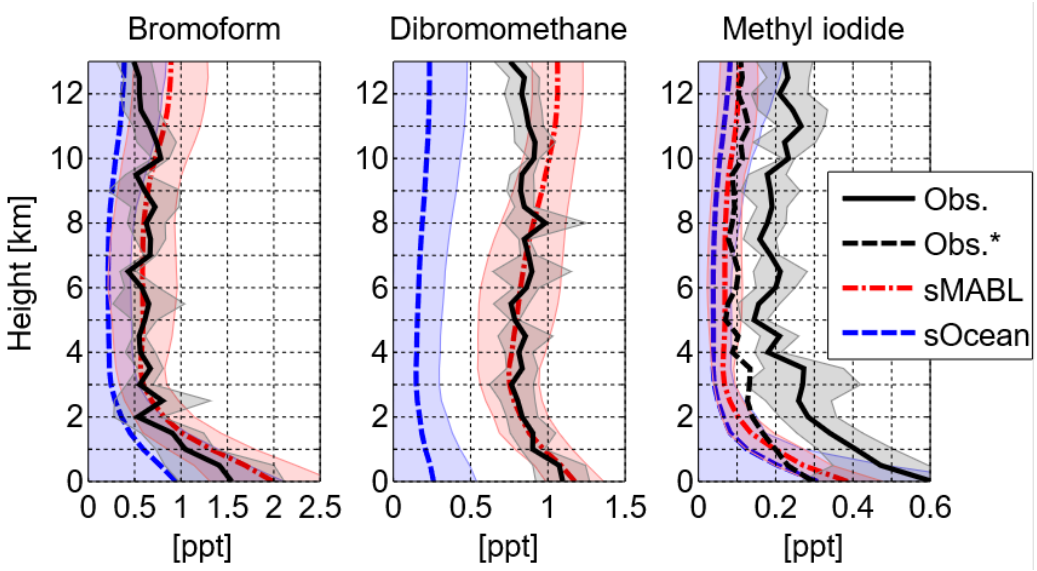

Figure 10: Mean FT mixing ratios (solid lines) and 1 standard deviation (shaded areas) from in-situ and flask observations on R/A FALCON (Obs~~v~~., black) versus simulated mean FT mixing ratios from MABL air (~~MABL~~sMABL, red) and oceanic emissions (~~Ocean~~sOcean, blue) observed by R/V SONNE. R/A FALCON in-situ observations have been adjusted for CH_3I (Obs~~v~~.*, dashed black) according to measurement deviations during the meetings of R/V SONNE and R/A FALCON (Table 2; Section 4.3).